



Araştırma Makalesi / Research Article

## Determination of Engineering Geological Conditions of A Plant-Site: A Case Study in an Open Pit Mine in Çine, Aydın

*Bir Tesis Alanının Mühendislik Jeolojisi Koşullarının Belirlenmesi: Örnek Çalışma, Çine, Aydın'da Yer Alan Bir Açık Ocak Feldspat Maden Sahası*

Saffet Deniz KARAGÖZ<sup>1</sup> , Mehmet Yalçın KOCA<sup>2\*</sup> 

<sup>1</sup>Dokuz Eylül Univ. Natural and Applied Sciences, Geological Engineering Dept. Buca-İzmir/TURKEY

<sup>2</sup>Dokuz Eylül Univ. Engineering Faculty, Geological Engineering Dept. Buca-İzmir/TURKEY

Geliş (Received): 27 Kasım (November) 2018 / Düzeltme (Revised): 08 Ocak (January) 2019 / Kabul (Accepted): 22 Ocak (January) 2019

### ABSTRACT

A plant will be constructed between the Alipasa and Sarıkısıç feldspar open-pit mines in Karpuzlu-Çine (Aydın) to conduct the works of crushing-grinding and flotation. An investigation was carried out to determine engineering geological conditions at and below the plant-site using scan-lines, geophysical measurements, and three inclined borehole data. Geological structure and ground conditions including geotechnical data such as discontinuity frequency and spacing, RQD% and CR% acquired from the drill hole exploration and geophysical survey are determined. Along the inclined drill holes, true discontinuity spacing values computed for each core run represent the most intersected discontinuities. In these calculations, determination of the acute angles between the axes of drill holes and strikes of the discontinuity sets are important as much as the investigation of fracture distributions in the subsurface. For this reason, the stereographic projection techniques were used to determine the true acute angle in this work. The purpose of the investigation is to identify and mitigate difficulties caused by ground conditions. The rock conditions comprise heavily jointed and weathered metamorphic rocks and the ability of these to support the foundations is considered. It was determined that the bearing capacity values obtained from the geotechnical computations considering RQD values agree with the ones acquired from the geophysical measurements, except the weakness zones (sheared zones). It was also determined that the values of allowable bearing pressure based on the geotechnical works are more conservative than the ones from the geophysical measurements. When all results are considered, the ratio between the allowable bearing capacity ( $q_a$ ) values acquired from geotechnical and geophysical measurements is close to 0.65.

**Keywords:** Site Investigation, Inclined Borehole, Geotechnical Data, Stereographic Projection, Geophysics, Bearing Capacity

### ÖZ

Karpuzlu, Çine/Aydın'da Sarıkısıç ve Alipaşa feldspat açık ocak madenleri arasında yer alan sahada kırma-öğütme ve flantasyon işlerini yürütmek için bir tesis inşa edilecektir. Hat etütleri, jeofizik ölçümler ve açılan üç eğimli sondajın verileri kullanılarak tesis alanında ve altındaki mühendislik jeolojisi koşullarını belirlemek için bir araştırma yapılmıştır. Jeofizik çalışması ve sondajlardan elde edilen süreksizlik sıklığı, aralığı, RQD ve karot verimi (CR) gibi jeoteknik verileri içeren yer koşulları incelenmiş ve sahanın jeolojik yapısı ortaya çıkartılmıştır. Eğimli sondajlar boyunca, en çok kesilen süreksizlikleri temsil eden her bir ilerleme için gerçek süreksizlik aralığı değerleri

*hesaplanmıştır. Bu hesaplamalarda, süreksizlik setlerinin doğrultusuyla sondaj eksenlerinin arasındaki dar açıların belirlenmesi yer altındaki süreksizlik dağılımının araştırılmasında oldukça önemlidir. Söz konusu gerçek dar açıların belirlenmesinde stereografik iz düşüm teknikleri kullanılmıştır. Araştırmanın amacı, yer koşulları nedeniyle ortaya çıkan zorlukları tanımlamak ve bu zorlukları en aza indirmektir. İnceleme alanı sık çatlaklı, ayrıışmış metamorfik kayalardan oluşmaktadır. Bu kayaların temel olma açısından bir değerlendirilmesi yapılmıştır. Makaslama zonları hariç, jeofizik ve RQD değerlerini dikkate alan jeoteknik yöntemlerle yapılan taşıma gücü analizlerinin sonuçlarının birbirleriyle uyumlu olduğu belirlenmiştir. Jeoteknik çalışmalar üzerine temellendirilmiş izin verilebilir taşıma gücü değerlerinin jeofizik çalışmalardan elde edilen değerlere göre; güvenli tarafta kalma açısından çok daha muhafazakâr sonuçlar verdiği ortaya çıkmıştır. Tüm sonuçlar dikkate alındığında, jeoteknik ve jeofizik ölçümlerden elde edilen izin verilebilir taşıma gücü değerlerinin oranı 0.65'e yakın bulunmuştur.*

**Anahtar Kelimeler:** Alan Araştırması, Eğimli Sondaj, Stereografik Projeksiyon, Jeofizik, Taşıma Gücü

## INTRODUCTION

The location of the site between the existing Alipasa and Sarıkısıık open-pit mines in Karpuzlu-Aydın, western part of Turkey is shown on Figure 1. The topography (platform) on which the plant will be built after the excavations is also shown on the cross-sections in Figure 2. It has been planned that the excavations will be made with depths reaching up to 26 m below the ground surface level (Figure 2). Three boreholes inclined up to 100 m. long were drilled in the plant site (BH-1, BH-2, and BH-3), (Figure 1). Declination angles (deviation angles from vertical) of the BH-1, BH-2, and BH-3 boreholes are 11°, 15°, and 45°, respectively. Geotechnical investigations are based on the ground conditions depending on the borehole data. The loggings of boreholes were performed and assessed from the geotechnical point of view. The rock quality designation (RQD %) and core recovery (CR %) values of the cores from which three inclined boreholes were obtained, were determined, and core losses (core loss =100 – CR %) were also computed for each length of core run.

The objective of the study involves exploring the ground conditions at and below the surface. This site investigation was performed to provide design information on: *i)* Three inclined boreholes were drilled in the plant-site. The boreholes were not only drilled to determine

the existence of the ore body, but also to find its vertical extent and to use it for mining purposes. In addition, geological structure and ground conditions including geotechnical data such as fracture frequency ( $\lambda$ ), spacing, RQD %, CR % acquired from the borehole exploration and from a geophysical survey. Thus, the zones of weakness beneath the foundation in terms of the fracture frequency were also determined. *ii)* Foundation bearing capacities of the rock units. The data utilised in engineering geology evaluations involved RQD %, CR %, and some mechanical properties. In this manner, the zones that are problematic in terms of bearing capacity were identified. The site investigation was undertaken to identify and mitigate difficulties that may arise during construction due to the ground conditions, and to mitigate risk associated with the crushing-grinding and flotation project.

Ground conditions were determined by drilling three inclined rotary boreholes to depths ranging from 100 m to 184.35 m (Figure 1). First aim of the borehole drills is to cut vertically the shear zone as much as possible because the albite ore body exists in this zone. It is required that the thickness of the albite ore body into the shear zone is determined in terms of mining operations. The boreholes were drilled to understand whether the thickness of ore body from the mining operations point of view is enough or not. The

orientations of boreholes are determined such a manner that they vertically cut the shear zone as much as possible without considering the in-situ distribution of other discontinuity sets in the subsurface. Second scope of the borehole drills is to investigate orientations of the discontinuity sets in the subsurface and to determine the acute angles between the borehole axes and the joint

sets to find true discontinuity spacing values of the sets. The boreholes were drilled along the geophysical measurement lines (line-1, line-2, and line-3) to match the results each other acquired from both methods (Figure 1). BH-2, BH-3, and BH-1 are located on the line-1, the line-2, and the line-3, respectively.

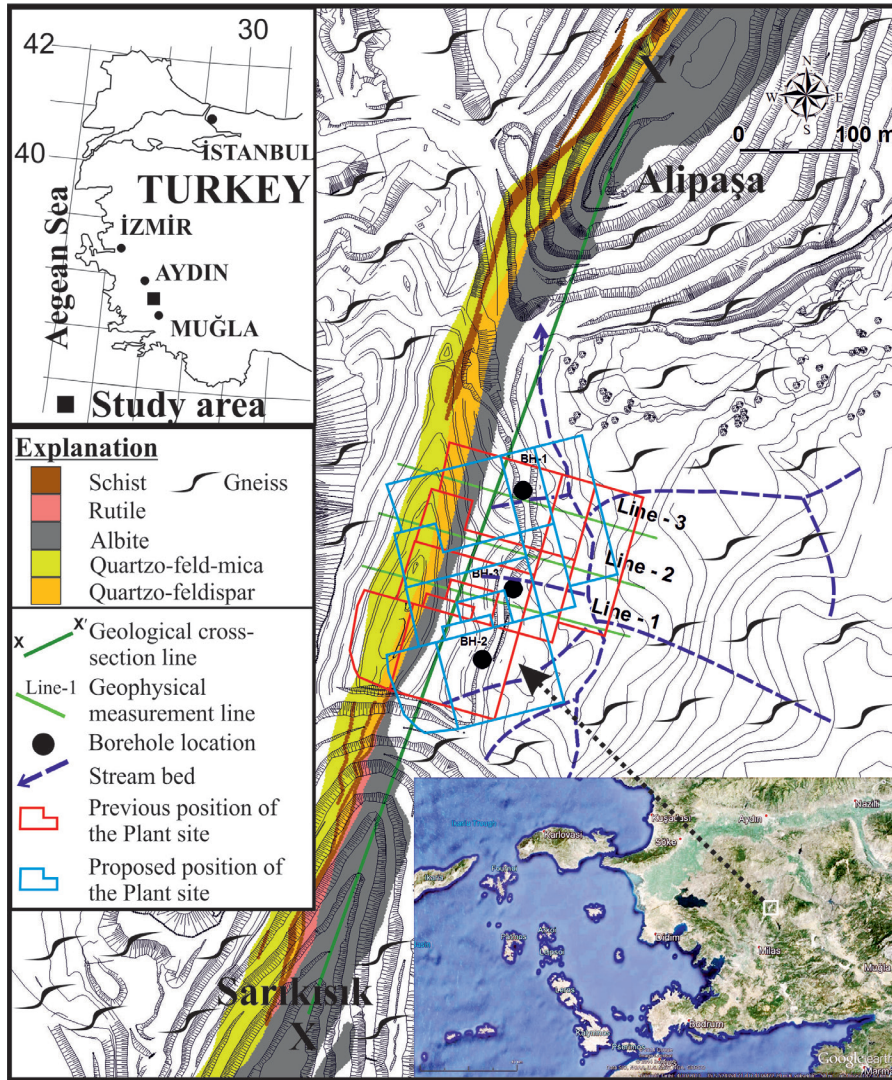


Figure 1. Geological and location map of the plant-site, general topographic conditions of the area, borehole locations and geophysical measurement lines.

Şekil 1. Tesis sahasının lokasyon ve jeoloji haritası, alanın genel topoğrafik koşulları, sondaj lokasyonları ve jeofizik ölçüm hatları.

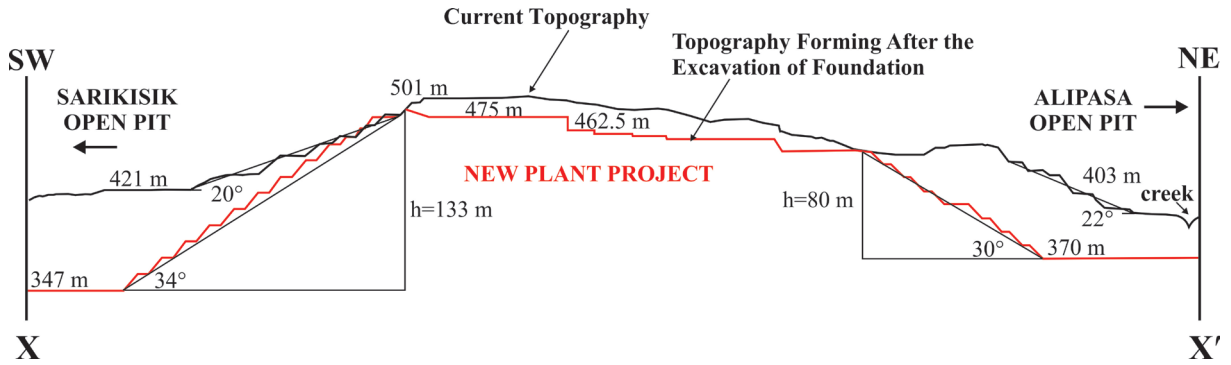


Figure 2. Current topography and the topography forming after the excavation of foundation.

Şekil 2. Güncel topoğrafya ve temel kazısı sonrası oluşan topoğrafya.

While the trends of borehole axes are the same (N70W), plunge angles of them are different from each other. The axis of each drill hole and the joint sets on the stereographic net are considered as a linear element and planar element, respectively. Determination of the acute angle between the axis of drill hole and strike of the discontinuity sets is important in terms of the investigation of fracture distributions in the subsurface. Orientations of the joint sets and shear zone (weakness zone) trending in nearly N-S direction in the plant site have been already known from the scan-line works which will be given in the following sections. In here, what is unknown is the thickness of which is variable along the length of it due to the shear deformation. In this point, the problem is reduced to find the acute angle between a linear element (borehole axis) and a planar element (discontinuity planes). For this reason, the stereographic projection technique was used to determine the true acute angle in this work. The problems involved in interpreting borehole data such as mathematical relationships, the strictly graphical techniques, and the stereographic projection technique. The problems can be solved much more rapidly on the stereographic projection net. It is determined that there are three problems to be solved about the fracture patterns in 3D; *i*) Which discontinuity

set, the value of fracture frequency at any core advance was computed for? Four different discontinuity types were identified during the site investigation works; 1. Discontinuities of the shear zone, 2. Joint sets, 3. Foliations, 4. Mica veins. *ii*) Which discontinuity set was mostly cut along the inclined borehole? *iii*) What are the acute angles between the shear zone, four discontinuity sets and the axes of the drill holes? Three inclined boreholes and the topography of the plant-site were loaded to the Micromine (2014) software. The software provides a useful and straightforward way to investigate fracture distributions in the subsurface in 3D. Thus, the orientations of the discontinuity sets, foliations, shear zone, inclined boreholes in three dimensions (isometric view), and the angular relations with each other were obtained.

The bias introduced by sampling discontinuities along lines, cylinders, and planes has been investigated by such authors as Terzaghi (1965), Priest (1994), Martel (1999), Zhou and Maerz (2002), Haneberg (2009). Martel (1999) developed a particular model for in situ distribution of fractures to analyze fracture pole orientations distributed on a hemisphere, with borehole bias being accounted for. Thus, one can not only predict the distribution and statistics

of fractures poles at a borehole survey but also modify the model based on the mismatch between observations and predictions. This approach presented by Martel (1999) provides a useful way to investigate fracture distributions in the subsurface. Zhou and Maerz (2002) and Haneberg (2009) indicate that the best strategy is to select a combination of different borehole orientations that minimizes the changes that average orientation of any discontinuity set falls into “a blind zone”. The prediction of statistical distribution of fractures’ poles at a borehole survey is beyond the scope of this paper. However, boreholes predominantly intersecting certain joint set /sets were determined using the stereographic projection techniques in this work.

Whether which discontinuity set mostly cut along the inclined borehole or cannot be determined before the borehole planning by using the projection techniques. For this aim,

there are two ways; a) Determination of true acute angle between axis of inclined borehole (linear element) and discontinuity set (planar element). If the true acute angle increases (if it is close to  $90^\circ$ ), mostly discontinuity intersects along the inclined borehole, b) Drawing the blind zones around the inclined boreholes. Discontinuity separated from boreholes by angles of  $30^\circ$  or less fall into “a blind zone”. Discontinuity data relevant to the discontinuities fall into this zone are difficult to interpret. As shown by Terzaghi (1965), discontinuities separated from boreholes fall into “a blind zone” and are likely to be statistically under-represented or completely missed in subsurface exploration programs. Subsequent authors confirmed her conclusion. A single inverse technique was described by Terzaghi (1965) in order to reduce this observational bias. If the Figure 3A is rotated at an angle of as much as “ $90^\circ$ - plunge angle”, the case of Figure 3B is obtained .

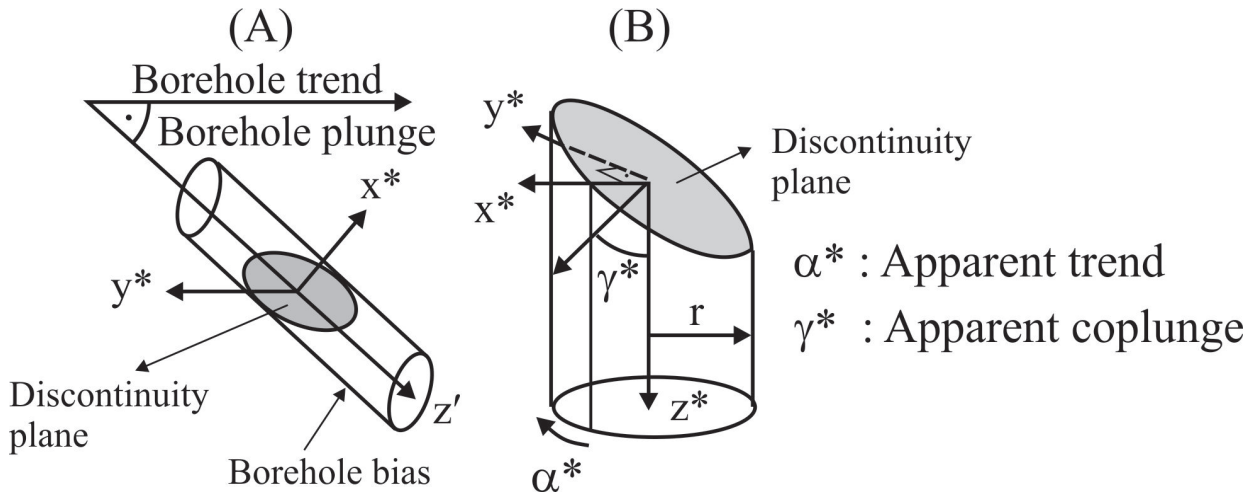


Figure 3. Representation of a discontinuity plane intersecting a borehole (modified from Martel, 1999).

Şekil 3. Bir sondajı kesen süreksizlik düzleminin gösterimi (Martel, 1999'dan değiştirilerek).

The value of true discontinuity spacing for each set was considered in bearing capacity numerical analyses of the weathered metamorphic rock. Bearing capacity is an important factor for the design of engineering structures, particularly when large rock masses are the foundation material (El-Naga, 2004). Bearing capacity values and stresses induced by the bearing loads were determined for heavily-jointed and weathered metamorphic rocks at the site. Bearing capacity analyses were performed using geotechnical methods that utilise RQD values and geophysical method proposed by Tezcan et al. (2006). These methods are suggested by Peck et al. (1974), Bowles (1988; 2001). The factor of safety in the first, second and third methods should be somewhat dependent on RQD %. RQD % is used to reduce the ultimate bearing capacity. Safety factor for rocks is selected between 3 and 6 (Bowles, 1988). This value for soils is selected between 2 and 3. The foundation response and bearing capacity of rock mass near ground surface is greatly influenced by discontinuities and their orientations. On the other hand, the zones with low RQD values indicate the weakness zones under the foundation in rock media. These zones which are in a discontinuous nature and have very high fracture frequency are problematic in terms of bearing capacity due to the low shear strength parameters developed depending on fracturing. Maximum foundation pressure is assigned to the bunker-hopper (width: 6.05 m, length: 6.3 m) which is a unit of the plant (0.51 MPa  $\approx$  51 ton/m<sup>2</sup>). Other units of the plant will apply lower pressures than the one of bunker.

## GEOLOGY

The geology of the plant-site and its surrounding area is dominated by the gneisses. Gneisses are characterised by their massive

structure. The ore bearing zone with a mineralogical composition of Na-feldspar was developed along the shear zone trending NE-SW in the area (Figure 1). It is seen that three rock units crop out in the site: ore body, quartzite-feldspar zone (tectonic zone, shear zone), and gneiss. In addition, mica zones are also seen along the contacts between the quartzite-feldspar zone and the gneiss unit (Figure 1 and 4).

The tectonic zone contains features such as quartzite lenses, rutile and thin mica veins, and albite ore body. Orientation of the albite ore body was determined from the geological investigation performed in the Alipasa open-pit beforehand (Kadağcı, 2011; Koca et al., 2014). Orientation of the ore body (N20-25E/50-70SE) in the plant-site, which locates in the middle of the pits, remains the same (Figure 1). The long axis of the plant is also trending along the same direction. Ore bearing zone was developed along the shear zone with 2.5 km length in the field. For this reason, there are discontinuities with nearly vertical position in both sides of the shear zone. However, the thicknesses of heavily fractured zones present in both sides of the shear zone are not well-known. The thickness of this zone varies due to the structural deformation (Figure 4).

Geological cross-sections were prepared using the borehole data and geological map of the plant area (Figure 4). The A-A', C-C', and E-E' geological cross-section lines are fitted to the geophysical measurement line-1, line-2, and line-3, respectively (Figure 1). In addition, the new topography resulting from the planned excavation works is recorded on these cross-sections. Foundation depths (elevations) of the units on the new topography are also illustrated on the cross-sections (Figure 4).

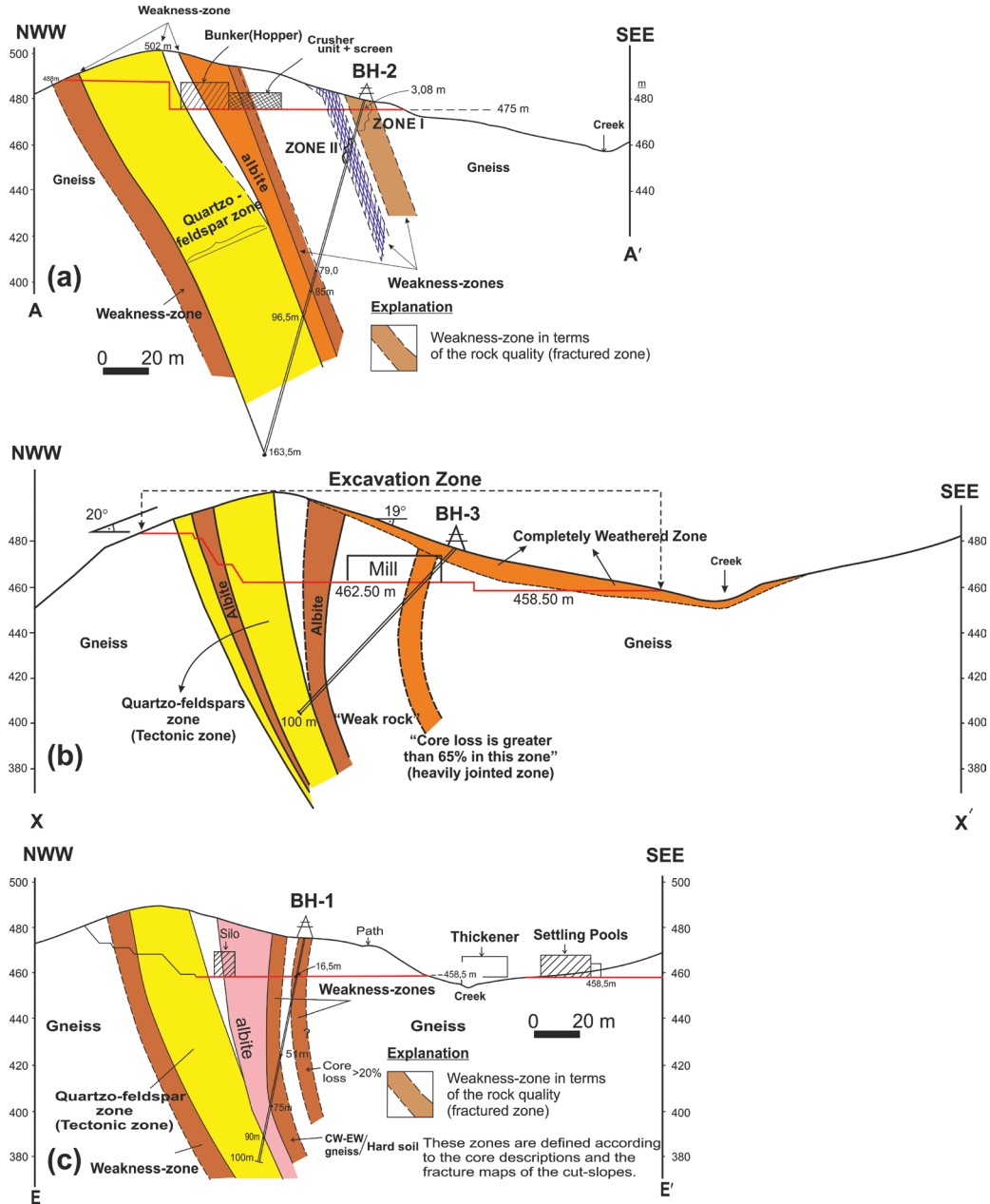


Figure 4. (a) The weakness zones placed at different depths along the BH-2 borehole profile and the locations of some units of the plant (A - A' cross-section), (b) The C - C' cross-section showing the heavily jointed rock zone along the BH-3 borehole, (c) The weakness-zones at different depths along the BH-1 borehole profile and the locations of some units of the plant (E - E' cross-section).

Şekil 4. (a) Tesisin bazı ünitelerinin lokasyonları ve BH-2 sondajının profili boyunca farklı derinliklerde yer alan zayıflık zonları (A - A' kesiti), (b) BH-3 sondajı boyunca yoğun çatlaklı kaya zonunu (gösteren C - C' kesiti), (c) BH-1 sondajı boyunca farklı derinliklerde gözlenen yoğun çatlaklı kaya zonu (zayıflık zonu) ve tesisin bazı ünitelerinin lokasyonları.

## METHODS

Field observations, discontinuity surveying including a quantitative description of discontinuities following ISRM (2007), core drilling and laboratory tests were undertaken in this study. Reliable determination of the main discontinuity orientations is very important in terms of the assessment of the subsurface geology. Discontinuity orientations were processed using Dips 6.0 (Rocscience, 2015). Orientations of the main discontinuity sets are determined from statistical interpretation of the discontinuity data acquired from the scan-line works. For this purpose, pole concentration points which represent the discontinuities are obtained by drawing the contour diagrams of the discontinuities by means of stereographic projection net. Thus, the number of joint sets and their orientations are revealed. To determine which discontinuity set will be intersected along the drilling directions of the boreholes are very important in terms of the true interpretation of each discontinuity set. In this work, boreholes predominantly intersecting certain tectonic joint set/sets were determined using the stereographic projection techniques because some boreholes predominantly intersect foliation planes and rarely intersect tectonic joint set/sets. In this case, along a certain borehole, fracture frequency and discontinuity spacing values computed for each core run represents the most intersected discontinuities.

Core samples obtained from the boreholes were investigated and assessed from geotechnical point of view. Discontinuity frequency ( $\lambda$ ), RQD %, and CR % (total core recovery) values were determined from the core samples. Core recovery as defined by ASTM D 2113 (1990) is the ratio between the length of recovered core and total

length of core run. The fractured rock mass is described using parameters such as discontinuity frequency ( $\lambda$ ) and discontinuity spacing ( $d$ ), etc. (Hudson and Priest, 1979; Stavropoulou, 2014);

$$\lambda = \frac{\text{No. of discontinuity}}{\text{logging interval}} = \text{No. of disc.} \times m^{-1} \quad (1)$$

Number of discontinuity was directly counted for each length of core run without considering the discontinuity orientation during the core logging. Intersected over an interval of length (the length of core run) along a borehole was only considered. Firstly, the aim in here is to find both the thickness of shear zone along the inclined boreholes and its depth from the ground surface. Secondly, the true thickness of shear zone is computed with help of the formula;  $x = y \times \text{Cos}\alpha$ . Where,  $x$  is the true thickness of weakness zone,  $y$  is apparent thickness of weakness zone, “ $\alpha$ ” is defined as the solid acute angle between the orientation of the borehole and strike of the shear zone.

It was noted by Terzaghi (1965) that the distance between discontinuities on a given discontinuity set along the length of a borehole depends on the orientation of the borehole relative to the discontinuities. For a set of extensive discontinuities having uniform discontinuity spacing,  $d$ , the number of discontinuities,  $N$ , intersected over an interval of length,  $L$ , along a borehole is;

$$N = \frac{L \times \sin\alpha}{d} \quad (2)$$

where, “ $\alpha$ ” is the acute angle between the strikes of discontinuity and the borehole’s axis as a linear element. For a vertical borehole, “ $\alpha$ ” equals the plunge of the pole point of discontinuity. Therefore, it is supposed that the interval

intersects a large number of discontinuities. Thus, a good approximation is acquired from the Equation 2. Using the angle instead of “ $\alpha$ ”, Equation 3 can be explained in a more general form useful for boreholes’ bias;

$$N = \frac{L \times \cos \gamma^*}{d} \quad (3)$$

where  $\gamma^*$  is the dip angle of discontinuity. The term of  $\cos$  in Equation 3 serves as a relative probability and ranges from zero to one ( $0 \leq \cos \leq 1$ ). Relative probability of intersecting a fracture where  $\alpha = 90^\circ$  (Borehole axis is just vertical to the discontinuity planes) ( $= 0$ ) is twice that where  $\alpha = 30^\circ$  ( $= 60^\circ$ ). A uniform change in the spacing between discontinuities or in their size changes the absolute probability of an intersection for an interval of length but not the relative probability  $\cos$  (Martel, 1999).

Terzaghi (1965) suggested that the discontinuities can be divided into groups of essentially the same orientation and the number of discontinuities in a given group,  $N$  (apparent), be replaced by (true),

$$\text{where } N^* = \frac{N_{app}}{\sin \alpha} \quad (4)$$

The term of “ $\frac{1}{\sin \alpha}$ ” in Equation 4 is a correction factor (it is also known as Terzaghi correction). The correction factor is large if “ $\alpha$ ” is small. Terzaghi contended that this should give a more representative picture of in-situ distribution of discontinuity orientations. In defining the number and size of groups of fractures with essentially the same orientation, and generally will not be a whole number. Also she cautioned against blind application of her inverse method for discontinuities nearly parallel to a borehole. She considered discontinuities oriented at less than  $30^\circ$  to a borehole to fall in

“a blind zone” where discontinuity data would be difficult to interpret. Equations 3 and 4 suggested by Terzaghi (1965) are used in order to determine the values of discontinuity spacing ( $d$ ) and fracture frequency ( $\lambda$ ) for each core run along the boreholes in this work.

Peck et al. (1974) suggested an empirical correlation between the rock quality designation (RQD %) and allowable bearing capacity stress ( $q_a$ ), which has a significant influence on the bearing capacity of a rock mass as given in Equation-5. Peck et al. (1974) is a commonly used method, however it is not considered appropriate for detailed design. The RQD has no meaning in terms of bearing capacity evaluations mechanically at a certain level. For this reason, second method proposed by Bowles (1988) is also used in this study.

$$q_a = 1 + \frac{(RQD/16)}{1 - (RQD/130)} \quad (5)$$

The relationship between ultimate bearing capacity (and RQD is made meaningful by means of Equation 6 suggested by Bowles (2001). The second method proposed by Bowles (2001) is based on a limit equilibrium expression for the ultimate bearing capacity of strip footings (Equation 7). The method considers the strength parameters of rock ( $c$ ,  $\phi$ ) and RQD values obtained from core logging (Equation 6). This method can be useful in terms of comparing the  $q_{ult}$  values for various foundation types obtained from the other empirical equations considering the RQD values.

$$q'_{ult} = q_{ult} \times (RQD)^2 \quad (6)$$

$$q_{ult} = \frac{1}{2} \gamma \times B \times N_\gamma \times S_\gamma + c \times N_c \times S_c + \bar{q} \times N_q \quad (7)$$

where,  $S_c$  and  $S_\gamma$  denote the Terzaghi shape factors,  $S_c = 1.3$  and  $S_\gamma = 0.6$  for the circular foundation,  $S_c = 1.12$  and  $S_\gamma = 0.85$  for the

rectangular foundation,  $N_c$ ,  $N_q$ , and  $N_\gamma$  are the bearing capacity factors for rocks,

$$N_c = 5. \tan^4 \left( 45 + \frac{\phi}{2} \right),$$

$$N_q = \tan^6 \left( 45 + \frac{\phi}{2} \right),$$

$$N_\gamma = N_q + 1, \quad (8)$$

$\bar{q}$  = vertical stress at the base of foundation,  $q_{ult}$  is the value of ultimate bearing capacity of rock (Merifield et al. 2006; Saada et al. 2008), and  $q_{ult}'$  is the reduced ultimate bearing capacity of the rock. Bowles (1988) proposed Equation 8 also based on

$$\text{RQD}\%: q_{ult} = q_r \times (\text{RQD})^2 \quad (9)$$

The term of “ $q_r$ ” in the Equation 9 is the ultimate strength of rock material determined by uniaxial compressive strength test. Some physical and mechanical properties of the gneisses, ore body, and the zones with mica (micaceous material) were determined by laboratory tests performed according to the suggestions by ISRM (2007).

Numerical analysis was also performed by using Phase<sup>2</sup> software (Rocscience, 2010) in order to compare the values of allowable bearing capacity computed from the empirical equations considering RQD-value and geophysical measurements. The rock mass was modelled based on the Generalized Hoek-Brown Criterion and the joint sets were imported with regard to the Mohr-Coulomb Criterion.

Geophysical surveys were planned along the profiles that intersect both the plant-site and the shear zone (Figure 1). Geophysical measurement lines were selected at nearly vertical position to the shear zone due to the unknown thickness of heavily fractured zones (weakness zones) present in both sides of the shear zone. The ore body and

the shear zone trends along N 25 E direction in Alipasa and Sarıkısıık open-pits (Koca et al., 2014). This geological structure having a large lenticular mass (a dome-like structure) is confirmed by the current study. In addition, the trend of the shear zone in the N 25 E direction is observed in both the benches of the adjacent mine slopes and the ground surface of the plant-site. The thickness of weakness zones in lateral direction (NW-SE direction) in the gneiss rock mass in the plant site is unknown. Different geophysical methods were applied in this study; the first one is the reciprocal method, and the second one is multi-channel analysis of surface waves (MASW method). The first method is focused on the analysis of structural changes in lateral direction in the field. This method considers the compression wave velocity ( $V_p$ ), (Palmer, 2001). The second method (MASW) is one of the seismic survey methods for evaluating the elastic condition of the ground for geotechnical engineering purposes. Shear wave velocity ( $V_s$ ) is a direct indicator of the ground strength (stiffness) and is therefore commonly used to derive load-bearing capacity, especially on rocky formations; the empirical expression given in Equation 10, (Tezcan et al., 2006) is used. In Equation 10,  $S_v$  is a reduction factor for materials in which shear wave velocities are greater than 500 m/sec (Equation 11).

$$q_{all} = 0.024 \times \gamma_n \times V_s \times S_v \quad (10)$$

Where  $\gamma_n$  is equal to  $[0.44 \times V_s^{0.25}]$ .

$$S_v = 1 - 3 \times 10^{-6} \times (V_s - 500)^{1.6} \quad (11)$$

Although, the empirical expressions of Equation 10 are proposed by the writers, on the basis of extensive geotechnical and geophysical soil investigations at 14 different sites, they should be used with caution. For relatively important buildings, and especially until a stage

when the validity of these simple empirical expressions are amply tested and calibrated over a sufficient period of time, the allowable bearing pressure should be determined also by means of conventional methods considering the bearing capacity factors for rocks.

### ENGINEERING GEOLOGICAL CONDITIONS OF THE SITE

Firstly, discontinuity scan-line surveys were performed at the site, and the results of

this work are presented in Table 1. The shear zone (tectonic zone) with the properties of the closely-jointed rock mass is trending in a nearly NW-SE direction at the plant-site (Figure 5). The zone has a problem from the perspective of the bearing capacity (Figure 5). Generally, this zone does not behave as a rock mass; in contrast, the zone behaves like a transitional material between weak rock and stiff to very stiff silty clay soil due to closely and very closely spaced discontinuities (Table 1).

Table 1. Quantitative descriptions and statistical distributions of discontinuities of tectonic zone at the plant site.  
*Çizelge 1. Tesis sahasındaki tektonik zona ait süreksizliklerin istatistiksel dağılımları ve sayısal tanımlamaları.*

Range	Description	Distribution (%)	
-	-	Gneiss	Quartzo-feldspar zone with thin mica veins (shear zone)
Spacing (mm)			
< 20	Extremely close	03	04
20-60	Very close	10	20
60-200	Close	40	68
200-600	Moderate	47	?
Persistence (m)			
3-10	Medium	60	34
10-20	High	24	58
> 20	Very high	16	?
Aperture (mm)			
0.25-0.50	Partly open	26	49
0.50-2.5	Open	55	31
2.5-10	Moderately open	19	20

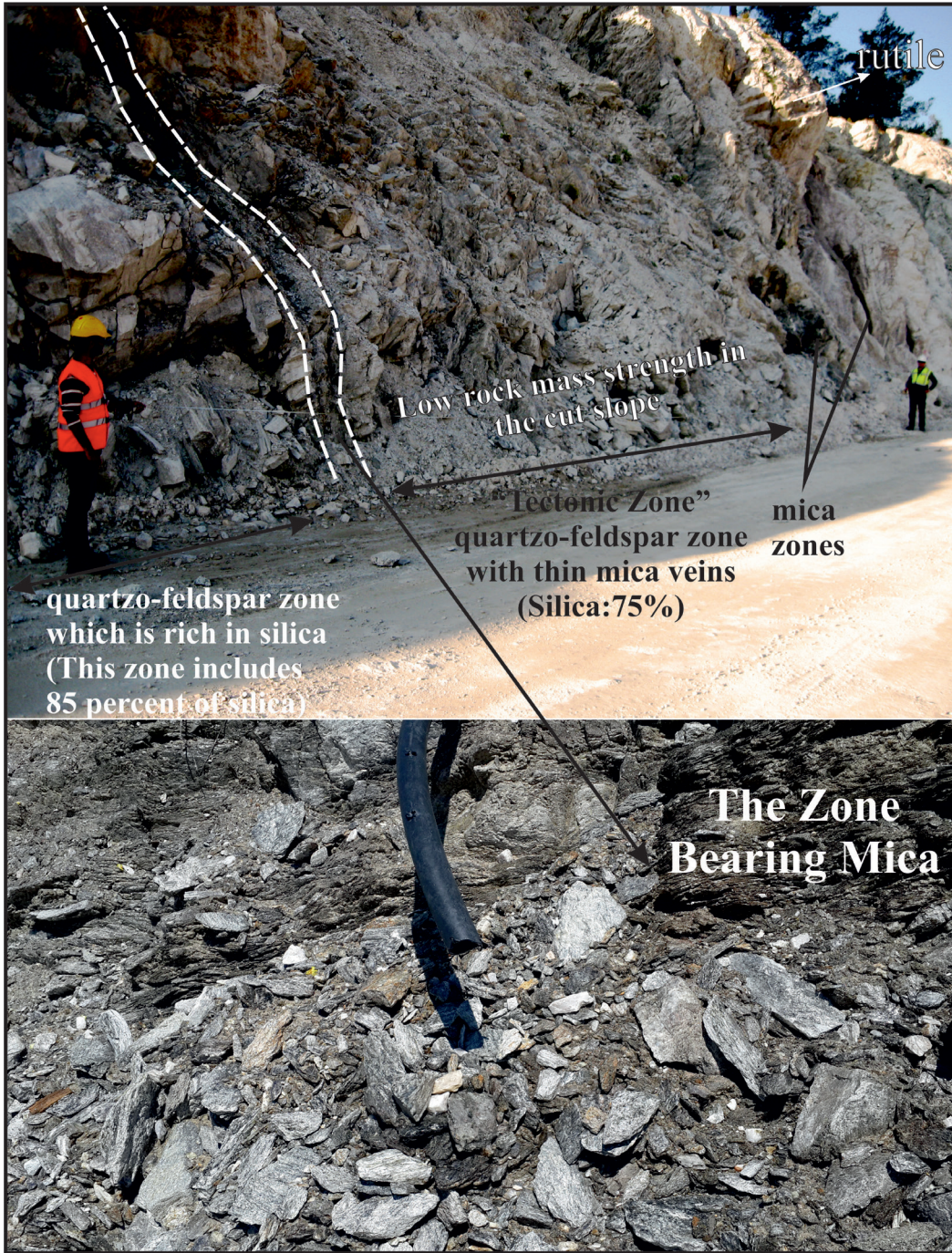


Figure 5. Relationships between the contacts of quartz-feldspar, mica zones and the tectonic zone on the cut-slope located at the Sarıkısık side.

Şekil 5. Kuvarso-feldspatik zon, mikalı zon ve Sarıkısık tarafında yer alan şev basamağı üzerindeki tektonik zon arasındaki ilişkiler.

Secondly, 440 discontinuity measurements were taken from the eastern and southern slopes of the plant-site. Initially, a contour diagram was prepared using all of the discontinuity data (Figure 6). Afterwards, the contour diagrams belonging to the eastern and southern slopes were prepared separately (Figure 7a and b). It is understood from the discontinuity measurements that there are four discontinuity sets that intersect one another.

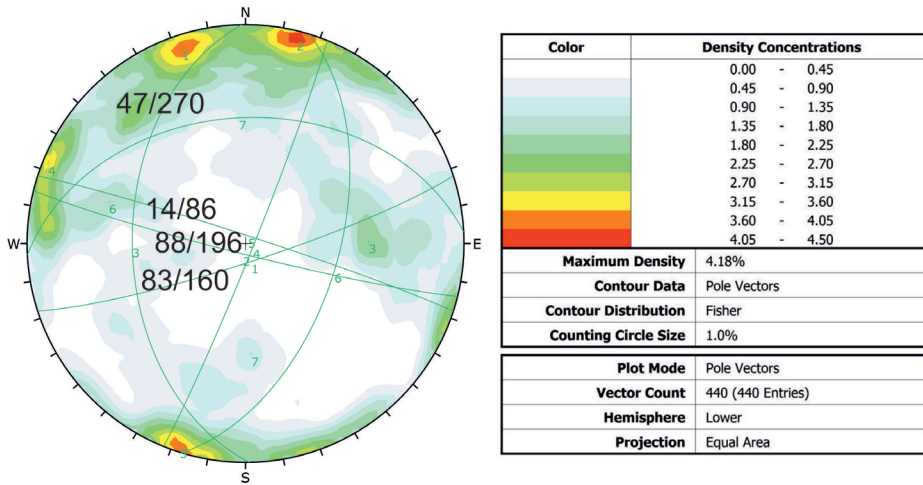


Figure 6. Contour diagram prepared using total discontinuity measurements (440) from the plant area and pole concentration points.

Şekil 6. Tesis alanından alınmış süreksizlik ölçüleri (440) kullanılarak hazırlanmış kontur diyagramı ve kutup yoğunlaşma noktaları.

Strikes of the discontinuities forming the pole concentration points, (and vertically cut into the long axis of the plant-site, and slopes are located at both sides of the site. However, strikes of the discontinuities forming the - pole concentration point are parallel to the long axis of the plant. Orientations of the main discontinuity sets affecting the bearing capacity values and stresses induced by surcharge loads are described below. This case is important in terms of the shear strength of discontinuities affecting the bearing capacity of the rock mass beneath the foundation.

- I) 47-32/270 and 36/250 Foliations with slightly undulated- smooth surfaces.
- II) 52/21, 86/14 Strikes of the joint sets are the same but their dip directions.
- III) 88/196 Both of them can be considered as one joint-set.
- IV) 65-83/160, 78/342 Both of the joint sets can be considered as one joint-set due to having similar strikes and different dip angles.
- V) 82 / 294

The X-X' geological cross-section with a NE-SW direction (Figure 8) was constructed to investigate fracture distributions in the subsurface. Set of joints appearing in this cross section are very important in terms of the determination of whether the sliding failure from the joints occur beneath the foundation under the axial stress condition or not. It should be noted that the shear stress caused of failure reaches the maximum value when -angle is equal to 45°.

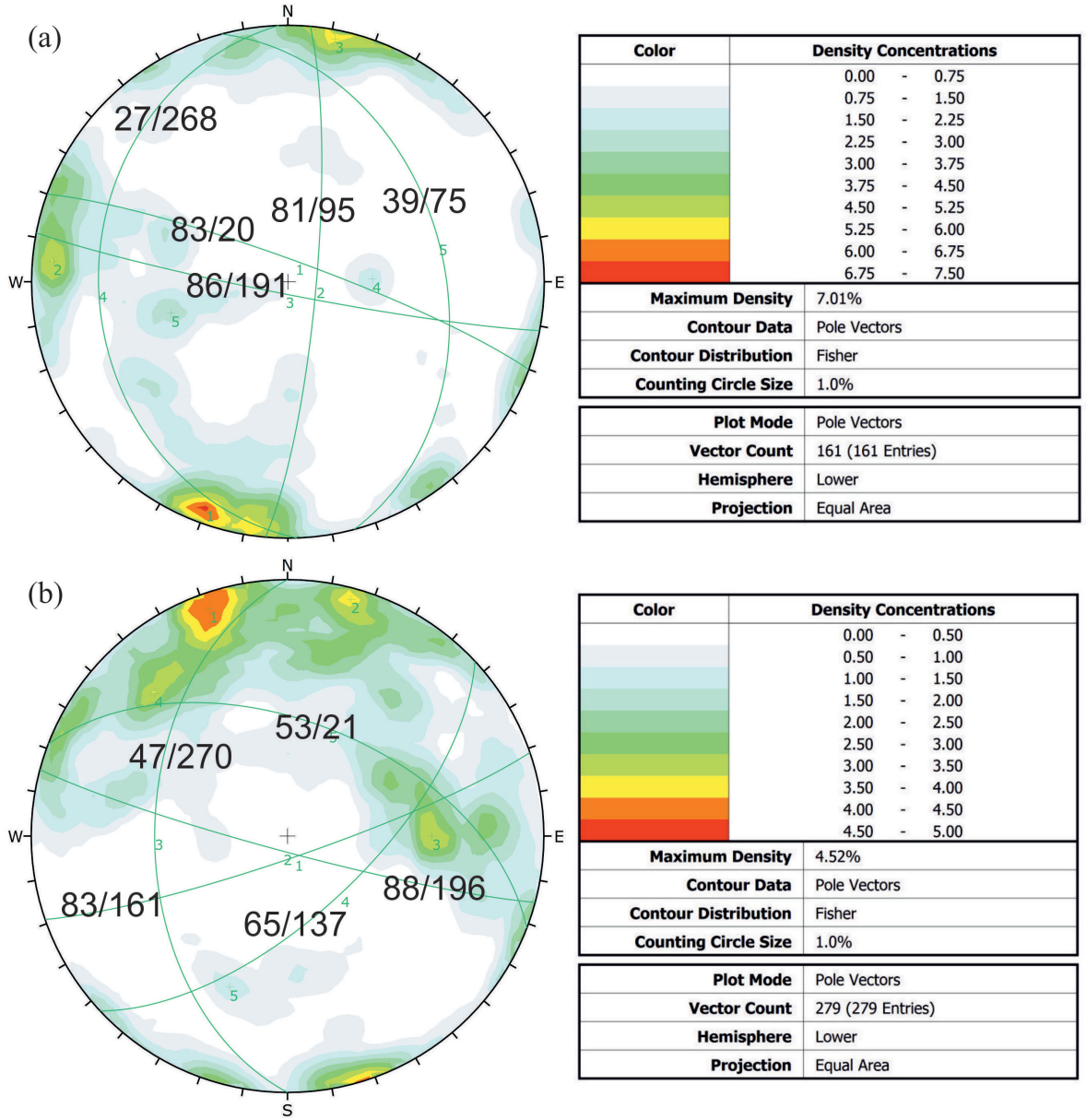


Figure 7. (a) Contour diagram prepared using the discontinuity measurements (161) from the eastern part of the plant area; (b) Contour diagram prepared using the discontinuity measurements (279) from the southern part of the plant area.

Şekil 7. (a) Tesis alanının doğu kesiminden alınmış süreksizlik ölçüleri (161) kullanılarak hazırlanmış kontur diyagramı, (b) Tesis alanının güney kesiminden alınmış süreksizlik ölçüleri (279) kullanılarak hazırlanmış kontur diyagramı.

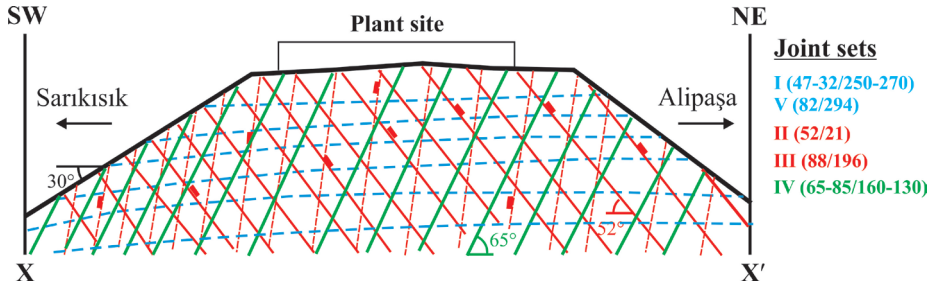


Figure 8. Discontinuity pattern along the X - X' cross-section line.

Şekil 8. X - X' kesit hattı boyunca süreksizlik ağı.

Foliations (set-I) and the discontinuities belonging to the set-V are stayed in nearly horizontal positions at the cross-section since the strikes of the cross-section line and the joint sets-I and V are parallel to each other Figure 8. For this reason, both of them are considered as only one joint-set. Discontinuities of the set-II appear at true dip angles, and their dip directions are towards to the Alipaşa mine. Dip directions of the discontinuities of the set-III lead to the slope-base at high dip angle. For this reason, they are not cut to the overall slope face. Set of joints appear along the X-X' cross-section line (Figure 8).

As a result of the surface water effect on the gneisses, the rock mass weathers to highly (HW) and/or completely weathered (CW) rock mass. On the other hand, the previously weathered or altered gneisses are affected by the present weathering process very quickly. Weathering changes the original colour of gneisses. Generally, gneisses show discoloration at the start of weathering. The discoloration usually starts

from the foliations and tectonic joint surfaces and extends inwards into the blocks. Porosity and microfractures of gneisses are increased by weathering. It is recorded an increase in porosity of as much as 34% in gneisses at advanced stages of weathering from moderately-highly (MW-HW) to highly-completely (HW-CW). The increase of 34% in porosity resulted in a decrease of 41.4% in strength of weathered gneisses (Table 2). In addition, the mean porosity and UCS values of moderately weathered (MW) gneisses are obtained as  $2.84 \pm 0.94$  (n=12) and  $27.34 \pm 5.30$  MPa (n=12, maximum 34.5 MPa, minimum: 23.0 MPa), respectively.

## LABORATORY TEST RESULTS

Bearing capacity analyses were performed using some physical and mechanical properties of the geologic units and discontinuity sets at the plant-site. Physical and mechanical properties of the gneisses, ore body, and the zones with mica, and three discontinuity sets were determined in the laboratory (Table 2).

Karagöz, Koca

Table 2. Physical and mechanical properties of gneiss, ore body, and micaceous material.

Çizelge 2. Gnays, cevher ve mikalı malzemelerin fiziksel ve mekanik özellikleri.

Some engineering properties of the gneisses, ore body, and weathered mica schist		Test results	
$\gamma_n$ (kN/ $\mu^3$ )	n: 6	25.0 $\pm$ 0.89	
n %	n: 6	3.42 $\pm$ 0.92	
$\sigma_c$ (MPa) (The gneiss unit with different weathering grades)		Unit weight ( $\gamma_n$ ): 0.0235 MN/m <sup>3</sup> Mean: 10.0 $\pm$ 1.50 (n = 7) Maximum: 12.0, Minimum: 8.0 Weathering grade: CW-HW	Unit weight ( $\gamma_n$ ): 0.025 MN/m <sup>3</sup> Mean: 17.06 $\pm$ 2.19 (n = 7) Maximum: 20.4, Minimum: 14.0 Weathering grade: HW-MW
$\sigma_c$ (MPa) (The orebody)	n: 4	Unit weight: 0.027 MN/m <sup>3</sup> Mean: 75 $\pm$ 12.5 “strong rock” in the R4-grade Maximum: 89.4, Minimum: 60.5	
		Foliation Planes	Intact rock material
Shear strength parameters according to the Mohr - Coulomb failure envelope ( $c'$ , $\phi'$ )		$\phi' = 36^\circ$ $c' = 0.027$ MPa $\tau = 0.027 + \sigma \tan 36$ , $R^2 = 0.97$ , n=8	$\phi' = 41^\circ$ $c'_p = 0.05$ MPa $\tau = 0.30 + \sigma \tan 41$ , $R^2 = 0.99$ , n=6
			Micaceous material
			$\phi'_p = 30^\circ$ , $\phi'_r = 22$ $c'_p = 0.05$ MPa $\gamma_n = 0.021 \pm 0.0012$ MN/m <sup>3</sup> $\tau = 0.05 + \sigma \tan 30$ , $R^2 = 0.90$ , n=4

n: Test number

Rock mass strength of the gneisses in the field is generally much lower due to the abundance of mica-coated joints and micaceous parting planes. However, the shear strength of the discontinuities in all rock types indicates little cohesion, with friction angles ranging from 30° to 41°, depending on rock type and infilling. Shear strength parameters were obtained as cohesion (c) 0.05 MPa and internal friction angle (internal friction angle) 30° from shear strength tests performed on the samples taken from the zones containing mica (Table 2). The strength of a rock material is determined in the laboratory on representative standard samples. In the case of a closely-jointed and/or highly-weathered rock

mass, it is not possible to obtain a sample with suitable dimensions to represent the entire rock mass. Accordingly, the uniaxial compressive strength values of the gneisses were determined as a mean value of 10.0  $\pm$  1.5 MPa for the CW-HW gneisses and 17.06  $\pm$  2.19 MPa for HW-MW gneisses (Table 2). In addition, micaceous deposits in the contact between the gneisses and the quartzite unit, as a soft vein or parting planes, are transitional material between very weak rock (UCS < 1.25 MPa) and stiff to very stiff soil. Due to above-mentioned reasons, the elastic modulus ( $E_s$ ) of the micaceous deposits was estimated at 0,13 $\times$ 10<sup>6</sup> kPa (130 MPa) as like as silty soil material (Table 3). After that, the value of elastic

modulus was taken as 0.13 kPa for the numerical analysis. In addition, the bulk unit weight of this material was determined as  $0.024 \pm 0.0012$  MN/m<sup>3</sup> (Table 2). Input data of the discontinuity sets used in the numerical analyses is given in Table 4. The lower internal friction angle value as  $\varphi = 26^\circ$  was determined for the slightly undulated-smooth discontinuity surfaces belonging to the joint set-3. The value of friction angles both for the joint set 1 and 2 were also determined as  $36^\circ$ . As a result of the shear box tests (rock on rock), the values of cohesion of the discontinuities for the joint set-1, joint set-2, and joint set-3 were determined as 100 kPa, 150 kPa, and 150 kPa, respectively. These values are of great importance for the numerical analyses performed by using Phase<sup>2</sup> software.

### Drilling Strategy

First aim of the drilling strategy for this work is to determine the drilling direction such a manner that most nearly perpendicular to the shear zone and ore body trending nearly parallel to the shear zone. Second aim is to determine which discontinuity set will be intersected along the drilling directions of the boreholes. In this work, two different methods based on the stereographic projection techniques were used to provide the aims mentioned above; *i*) Drilling strategy including the determination of the acute angles between the discontinuity sets and axes of the boreholes. The acute angle determination method based on the fixing of the acute angle between linear and planar elements is a new approach in terms of the drilling strategy.

Table 3. Input data of the rock materials used in the numerical analyses.

*Çizelge 3. Nümerik analizlerde kullanılan kaya malzemelerine ait yazılım girdileri.*

Material parameters (input data)	Rock Units		
	Gneiss	Ore Body	Tectonic Zone
Unit weight (kN/m <sup>3</sup> )	25	27	24
Initial void ratio, e %	0.035	0.035	0.035
Deformation modulus (kPa)	$1.64 \times 10^6$	$1.24 \times 10^6$	$0.13 \times 10^6$
Poisson's ratio ( $\nu$ )	0.28	0.30	0.23

Table 4. Input data of the discontinuity sets used in the numerical analyses.

*Çizelge 4. Nümerik analizlerde kullanılan çatlak takımlarına ait yazılım girdileri.*

Number of joint sets	Joint plane-1	Joint plane-2	Joint plane-3
Dip/Dip direction	36/250	21/52	78/342
Cohesion (kPa)	100	150	150
Angle of friction ( $^\circ$ )	36	36	26

This method includes the numerical comparison of acute angle with the limitation of  $30^\circ$  of Terzaghi (1965). *ii*) Drilling strategy considering the plot of “blind zones” around the boreholes and great circles of the discontinuity sets (dip-lines). On the other hand, when these strategies are put forward, drilling cost should be also considered. As known, as the declination angle from the verticality of a borehole increases, drilling cost of it also increases. This case given above is considered in this work. In other words, the applications in the site were performed by reducing the drill angle of a borehole.

Declination angles of BH-1, BH-2, and BH-3 boreholes are  $11^\circ$ ,  $15^\circ$ , and  $45^\circ$ , respectively (Figure 4). The acute angles between trend of borehole axis and strikes of discontinuities should not be less than  $30^\circ$  according to the method suggested by Terzaghi (1965). If not, discontinuities belong to any joint set lie in “a blind zone” around a borehole. For this reason, acute angles between the borehole axes (the boreholes’ azimuths are the same - N70W but their plunge angles) and the discontinuity sets are determined by using the stereographic projection technique in this study. Angular relationships between the axes of the drill holes BH-3, BH-2 and bearings of the joint sets are determined as follows in Figure 9. While the BH-3 borehole cuts the shear zone and the discontinuities belongs to the joint set-4 (82/294), the BH-2 borehole cuts the shear zone and the foliation planes into the gneiss rock unit at different angles ( $35^\circ$  and  $40^\circ$ ) (Table 5, Figure 9 and 10). The acute angles between the shear zone and the axes of the drill holes BH-3, BH-2, and BH-1 are determined as  $65^\circ$ ,  $35^\circ$ , and  $31^\circ$ , respectively (Figure 10). The

acute angles for the foliation planes are also determined as  $16^\circ$ ,  $40^\circ$ , and  $44^\circ$ , respectively. It should be noted that the plunge angle of BH-3 borehole ( $45^\circ$ ) is far smaller than the dip angles of the discontinuities that belong to the joint sets.

The distance between discontinuities of a given set along the length of a borehole depends on the orientation of the borehole relative to the discontinuities. The plunge angle of borehole BH-3 (N70W/45NW) is quite close to the dip angles ( $26^\circ$ -  $42^\circ$ ) of the foliations. The acute angle between the strikes of the foliations and the axis of the BH-3 borehole is determined as  $16^\circ$  (Figure 10). This case given above decreases the probability of BH-2 borehole cut the foliation planes considerably (Figure 10). However, it was found that BH-2 borehole intersected the foliation planes and the shear zone (Figure 10). Foliation planes are cut along the BH-1 and BH-2 boreholes mostly. The discontinuities belonging to the joint set-4 are, on the other hand, cut along the BH-3 borehole mostly (Table 5). The borehole axes of BH-3 and BH-2 boreholes seem to be nearly vertical to the strike of the joint set-4 from Figure 9d. In addition, trend of the borehole axis (N70W) in 3D is nearly the same with dip directions of the discontinuities belonging to the joint set-4. For this reason, they cut each other at small acute angles such as  $36^\circ$  and  $7^\circ$  (Figure 9d). Acute angles between them are determined as to be fairly low on the stereographic net (Figure 9d). A similar case to the one given above is also seen for the joint set-3 (78/342). Acute angles between joint set-3 (planar element) and axes of the boreholes BH-3, and BH-2 are determined as to be  $16^\circ$  and  $2^\circ$ , respectively (Table 5, Figure 9c).

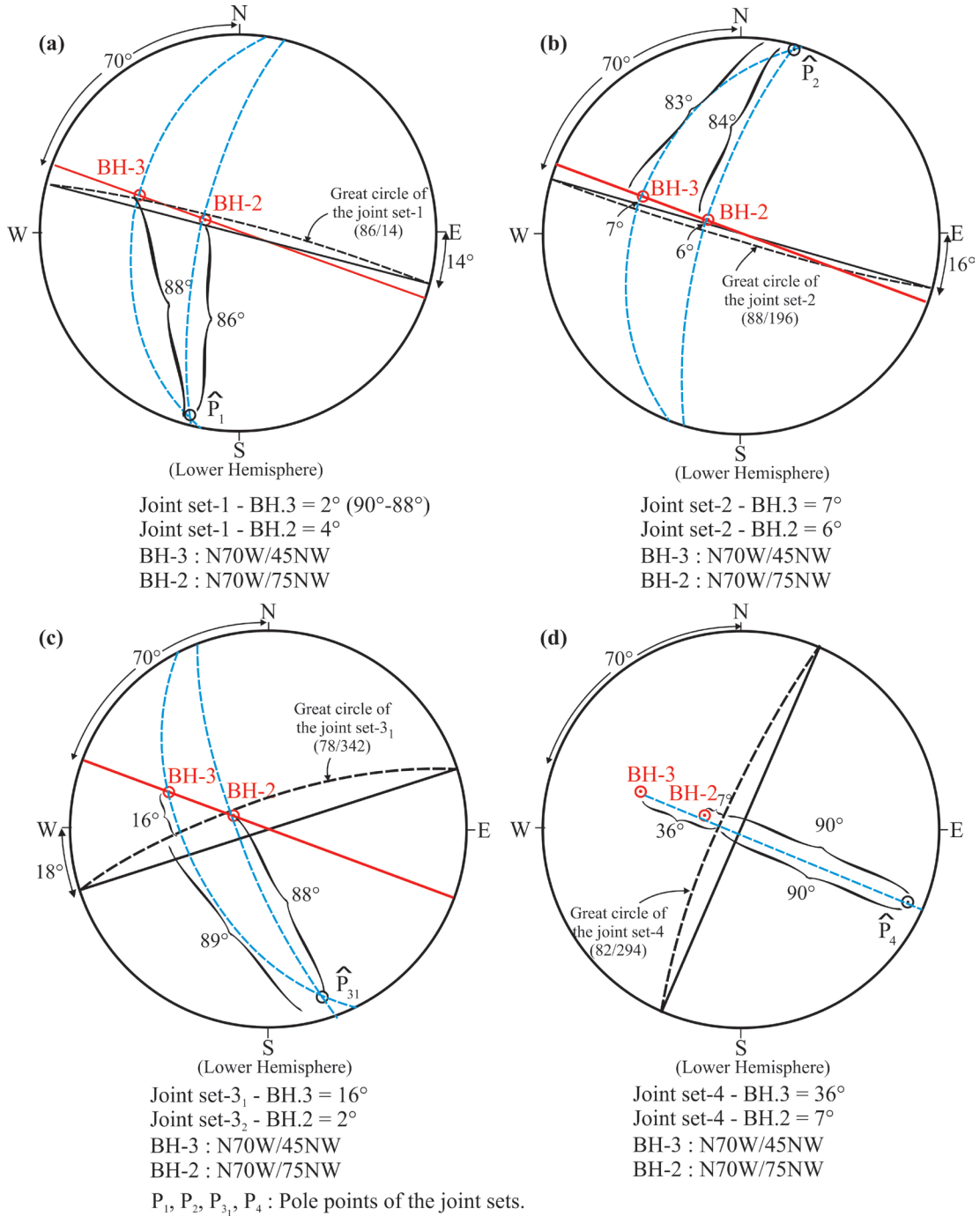


Figure 9. Determination of the acute angles between the borehole axes and the joint sets by means of the stereographic projection technique.

Şekil 9. Stereografik projeksiyon tekniği yardımıyla çatlak setleri ve sondaj eksenleri arasındaki dar açılarının belirlenmesi.

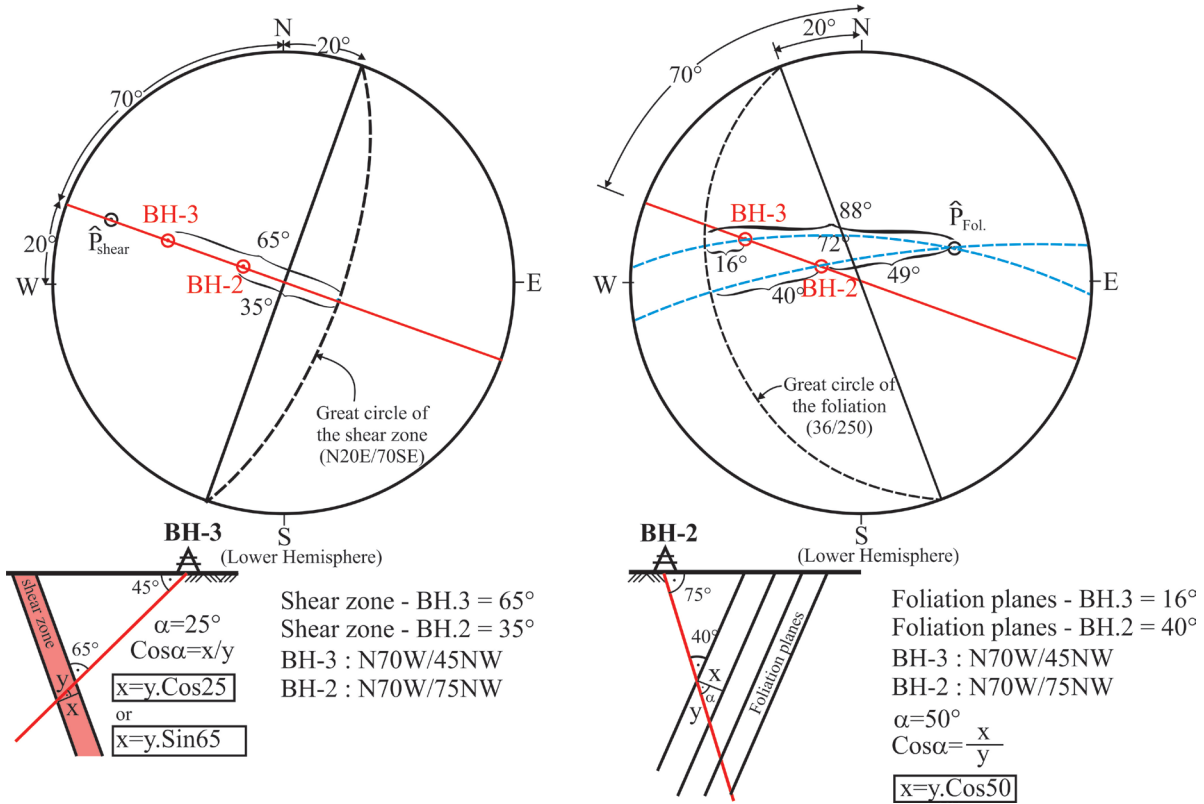


Figure 10. Determination of the acute angles between the borehole axes and the shear zone, and foliation plane by means of the stereographic projection technique.

Şekil 10. Stereografik projeksiyon tekniği yardımıyla foliasyon düzlemleri, makaslama zonu ve sondaj eksenleri arasındaki dar açılardan belirlenmesi.

It will be noticed that BH-2 and BH-1 boreholes intersect the shear zone and the foliation planes mostly. On the other hand, these boreholes cut rarely the discontinuity sets of 86/14 (set-1), 196/88 (set-2), and 78/342 (set-3) (Figure 9 and 10). On the other hand, these boreholes do not cut the discontinuities tagged as 86/14 (set-1) and 88/196 (set-2) since the trends of the axes of BH-2 and BH-1 drill holes are nearly parallel to the strikes of discontinuities belong to the joint set-1 and set-2 (196/88), (Table 5). In addition, BH-2 and BH-1 boreholes rarely cut the discontinuities belong to the joint set-4

(294/82) since the dip angles of joints are nearly equal to the plunge angles of the boreholes and trends of the boreholes are nearly parallel to the dip directions of the discontinuities. This case given above decreases the probability of getting cut of the discontinuities by the boreholes.

All angular relationships at and below the surface are noticed in Figure 11. Isometric views of the ground conditions which include the orientations of the discontinuity sets, shear zone, and inclined boreholes in 3D are presented (Figure 11).

Table 5. The acute angles between the borehole axes (linear elements) and the joint sets, the shear zone and the foliation planes (planar elements).

Çizelge 5. Sondaj eksenleriyle çatlak takımları, makaslama zonu ve foliasyon düzlemleri arasındaki dar açılar.

Type and orientation of discontinuity (dip direction/dip angle)	Orientation of borehole axis (azimuth/plunge)	Measured acute angle (a°)	Numerical comparison	Explanation
Shear zone (110/70)	BH-3 (N70W/45NW)	65	$a > 30^\circ$	Strike of the shear zone is exactly vertical the trend of borehole axis
	BH-2 (N70W/75NW)	35	$a > 30^\circ$	
Foliation plane (250/36)	BH-3 (N70W/45NW)	16	$a < 30^\circ$	BH-2 borehole cuts the foliation planes at a considerably angle (40°).
	BH-2 (N70W/75NW)	40	$a > 30^\circ$	
Joint set-1 (14/86)	BH-3 (N70W/45NW)	2	$a < 30^\circ$	The trend of borehole axis is nearly parallel to the strike of the discontinuity set. Boreholes rarely cut this set for each length of core run.
	BH-2 (N70W/75NW)	4	$a < 30^\circ$	
Joint set-2 (196/88)	BH-3 (N70W/45NW)	7	$a < 30^\circ$	
	BH-2 (N70W/75NW)	6	$a < 30^\circ$	
Joint set-3 <sub>1</sub> (342/78)	BH-3 (N70W/45NW)	16	$a < 30^\circ$	Boreholes rarely cut this set for each length of core run.
	BH-2 (N70W/75NW)	2	$a < 30^\circ$	
Joint set-4 (294/82)	BH-3 (N70W/45NW)	36	$a > 30^\circ$	The trend of borehole axis and the dip directions of discontinuities are nearly the same. The borehole intersects both the shear zone and joint set-4.
	BH-2 (N70W/75NW)	7	$a < 30^\circ$	

### Drilling Strategy Considering the Acute Angles Between the Axes of the Boreholes and Discontinuity Sets

The light gray circles represent  $30^\circ$  cones defining the blind zones (shadow zones) around the BH-3 and BH-2 inclined boreholes (Figure

12). Cones (Cone-1 and Cone-2) representing the shear zone intersected by the drill holes 2 and 3 are presented in Figure 12. The representation of these cones at the earth's surface is also presented in the same figure. The discontinuities separated from the boreholes by an angle of  $30^\circ$  lie in this zone.

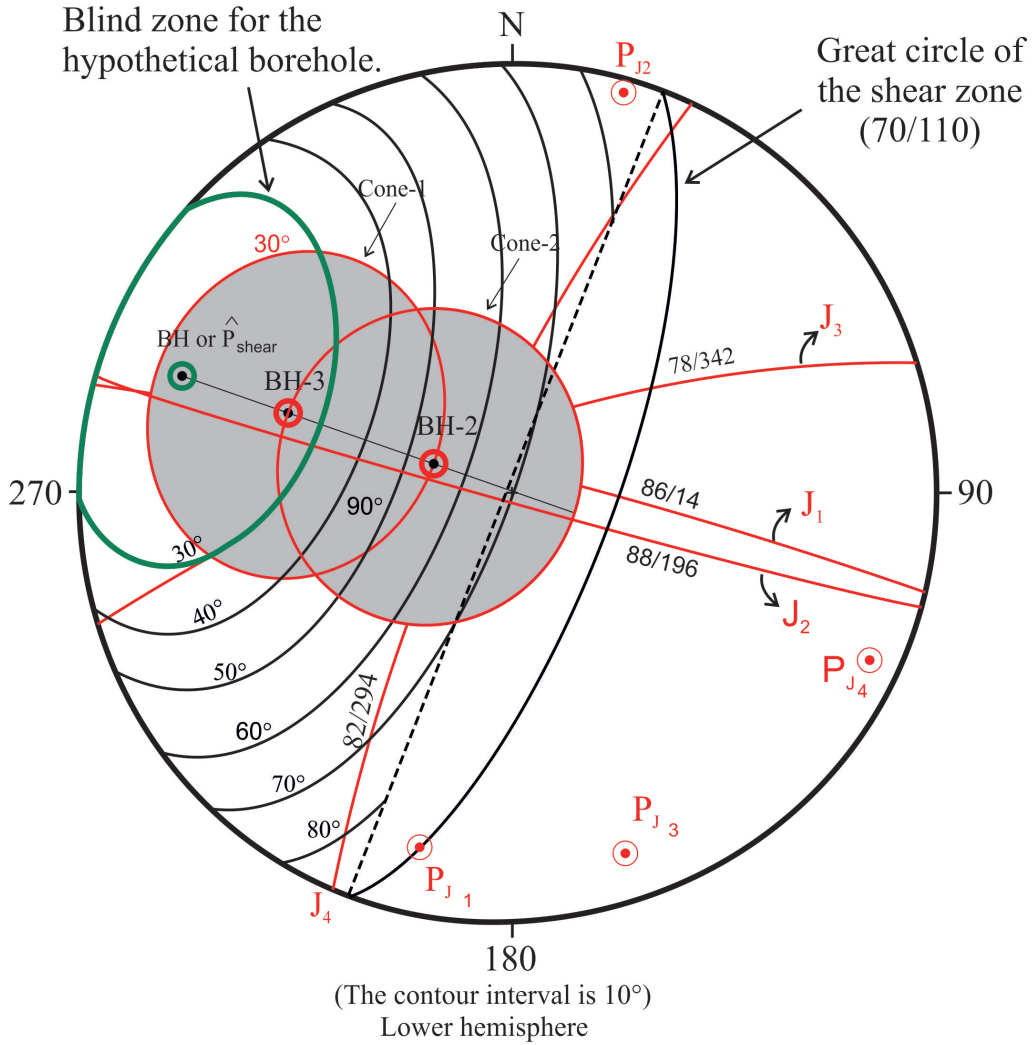


Except the shear zone and the joint set 4 (Joint set 4 – BH-3 =  $36^\circ$ ), the acute angles between the trends of boreholes axes and the strikes of the joint sets are determined to be less than  $20^\circ$  (Figure 12). If the borehole had just been drilled in this point, a single minimum at 20/290 (shear) for the shear zone (70/110) would have been produced according to the method suggested by Haneberg (2009) (Figure 12). In here, the drilling direction that is most likely to minimize bias is described as the minimum (20/290). Borehole bias is normal to a discontinuity in which case the borehole point and the pole point of discontinuity coincide. Minima are sought because they represent drilling directions that should produce the smallest aggregate difference between the borehole and the poles of the discontinuities. In this study, the most suitable drilling direction is that of the BH-3 borehole because orientation of the BH-3 borehole is more close to the point of shear than that of the BH-2 borehole. Lower hemisphere equal area projection illustrating a drilling strategy for the shear zone is represented in Figure 12.

It should be noted that the boreholes rarely cut the discontinuities belong to the joint sets due to the orientation of the boreholes relative to the discontinuities, except the case between the borehole axis of BH-3 and the joint set-4. The borehole axis of BH-3 cut at a certain degree the joint set-4 (acute angle:  $36^\circ$ ). The highest acute angle value is obtained as  $65^\circ$  from the relationship between the trend of BH-3 borehole axis and the shear zone. For this reason, the values of discontinuity spacing (d) and frequency

( $\lambda$ ) for each core run along the BH-3 borehole are determined according to the number of discontinuities, N, intersected over an interval of length, L, and acute angle ( $\alpha$ ) between the trend of BH-3 borehole axis and the shear zone (Table 7). In order to match the data acquired from both boreholes, the values of “d” and “ $\lambda$ ” for each core run along the BH-2 borehole are also determined (Table 6).

While the BH-3 borehole cut the shear zone at fairly high angle ( $65^\circ$ ), BH-2 and BH-1 boreholes cut both the shear zone and the foliation planes into the gneiss rock mass relatively at low angles ( $35^\circ$  and  $40^\circ$ ), (Table 6 and 7). As a result, of this case, much more number of discontinuity (discontinuity number: 143) is intersected along the BH-3 borehole than the ones (discontinuity number: 105) along the BH-2 borehole for the depth of 25.5 m from the ground surface level (Table 6). At depths ranging from the surface to 25.5 m for two boreholes, discontinuities are intersected at different number for each borehole due to the different acute angles between the trend of borehole axis and the strikes of discontinuities. For this reason, it is determined that the values of fracture frequency belonging to the BH-2 borehole for each core run are greater than the ones for the BH-3 borehole, except the shear zone (Table 6 and 7). BH-3 borehole cut more number of discontinuities at the ratio of 26.57 % than that of the BH-2 borehole. The values of fracture frequency along the shear zone are nearly the same for both boreholes because the zone has a rock mass including very closely spaced discontinuities.



$J_1, J_2, J_3, J_4$ : Great circles of the joint sets

$P_{j1}, P_{j2}, P_{j3}, P_{j4}$ : Pole points of the joint sets

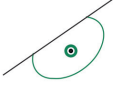
-  : Blind zones for the BH-2 and BH-3 boreholes.
-  : The case that a hypothetical borehole and pole point of the shear zone coincide.  
(The most suitable borehole location because angular deviation for the shear zone is minimum in the pole point of the shear zone ( $P_{\text{shear}}$ )).
-  ,  : ..... borehole (BH-3, N70W/45NW,  
: BH-2: N70W/75NW, BH: N70W/20NW)

Figure 12. Lower hemisphere equal area plot illustrating a drilling strategy for the shear zone and joint sets.

Şekil 12. Makaslama zonu ve çatlak takımları için bir sondaj stratejisini gösteren eş alan projeksiyonu.

Table 6. The values of discontinuity spacing and frequency for each core run along the BH-2 borehole (acute angle between the BH-2 borehole and the shear zone = 35°,  $\text{Cos } \gamma^* = 0.5725$ ).

Çizelge 6. BH-2 sondajı boyunca makaslama zonundaki her bir ilerleme için süreksizlik sıklığı ve süreksizlik ara uzaklığı değerleri (BH-2 sondajı ve makaslama zonu arasındaki derece 35°).

Core run (m)	L (m)	N*	N	d (cm)	$\lambda$ (m <sup>-1</sup> )	Joint spacing (ISRM 2007)
2 - 4	2	17.5	10	6.5	15.4	
4 - 7	3	16	9	10.7	9.3	
7 - 10.5	3.5	24.5	14	8.2	12.2	
10.5 - 13	2.5	10.5	6	13.6	7.3	
13 - 14.5	1.5	7	4	12.3	8.1	
14.5 - 17.5	3.0	17.5	10	9.8	10.2	
17.5 - 18.5	1.0	7	4	8.2	12.2	Close spacing (closely jointed rock mass)
18.5 - 20.0	1.5	9	5	9.5	10.5	
20.0 - 21.5	1.5	9	5	9.5	10.5	
21.5 - 24.0	2.5	10.5	6	13.6	7.3	
24.0 - 25.5	1.5	7	4	12.2	8.2	
25.5 - 27.0	1.5	9	5	9.5	10.5	
27.0 - 30.0	3.0	14	8	12.2	8.2	
30.0 - 31.5	1.5	10.5	6	5.4	18.5	Very close spacing
31.5 - 36.5	5.0	16	9	17.9	5.6	Close spacing
			105	10.6 ± 3.15	10.3 ± 3.33	

d: Discontinuity spacing =  $\frac{L \cdot \text{xcos}\gamma}{N}$ ,  $N = N \cdot \frac{1}{\text{sin}\alpha}$ ,  $\frac{1}{\text{sin}\alpha}$  = Correction factor.

Table 7. The values of discontinuity spacing and frequency for each core run along the BH-3 borehole (acute angle between the BH-3 borehole and the shear zone = 65°,  $\text{Cos } \gamma^* = 0.9063$ ).

Çizelge 7. BH-3 sondajı boyunca makaslama zonundaki her bir ilerleme için süreksizlik sıklığı ve süreksizlik ara uzaklığı değerleri (BH-3 sondajı ve makaslama zonu arasındaki derece 65°).

Core run (m)	L (m)	N*	N	d (cm)	$\lambda$ (m <sup>-1</sup> )	Joint spacing (ISRM 2007)
0 - 6.0	6.0	31	28	17.5	5.7	Close spacing
6.0 - 7.0	1.0	3.3	3	27.5	3.6	Moderate spacing
7.0 - 9.5	2.5	20	18	11.3	8.8	
9.5 - 12.5	3.0	21	19	12.9	7.8	
12.5 - 15.5	3.0	24	22	11.3	8.8	Close spacing
15.5 - 17.5	2.0	10	9.0	18.1	5.5	(closely jointed rock mass)
17.5 - 18.5	1.0	12	11	7.5	13.3	
18.5 - 21.5	3.0	17	15	16	6.2	
21.5 - 24.5	3.0	13	12	21	4.8	Moderate spacing
24.5 - 25.5	1.0	6.6	6	13.7	7.3	Close spacing
			143	15.7 ± 5.71	7.2 ± 2.74	

### Drilling Strategy Considering the Blind Zones

A drilling strategy for situation in which discontinuity orientation is unknown, was outlined by Terzaghi (1965). Two stereographic projections (stereograms) showing the right and the wrong drilling strategies are presented in Figure 13 and 14, respectively. Figure 13 and 14 show two lower hemisphere equal area projections with 30° blind zone for the inclined boreholes. Discontinuities for which dip-lines (defined by a dip and dip direction) fall into the blind zones for the boreholes are unlikely to be encountered in that boreholes. Those discontinuities will, however, be encountered in other boreholes as long as the blind zones do not overlap.

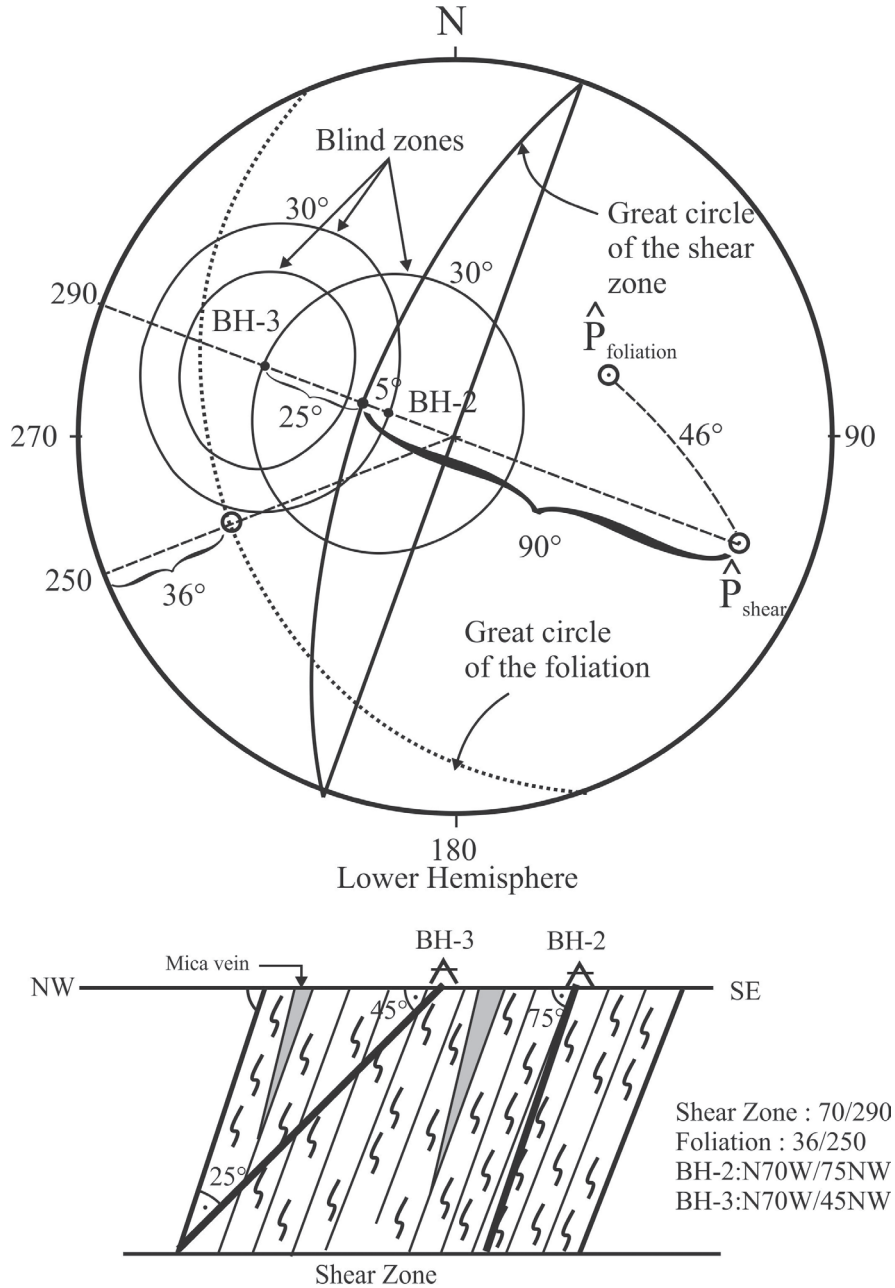
In the right strategy, position of the shear zone (shear zone:70/110) is considered as in Figure 13. On the other hand, if the dip direction of the shear zone had been rotated at an angle of 180° with the same strike, the inclined boreholes would not intersect the shear zone (wrong strategy) as illustrated in Figure 14 (shear zone: 70/290). There are two reasons to distinguish right and wrong strategies. *i)* While BH-2 borehole does not cut the shear zone in the wrong strategy, in the right strategy, the borehole cut the shear zone. *ii)* While BH-3 borehole cut very few numbered discontinuity in the shear zone in the wrong strategy, the borehole cut considerably the discontinuities in the shear zone, but as much as at BH-2 borehole in the right strategy. In the right strategy, the acute angle between BH-3 borehole and the discontinuities in the shear zone is 65° (Figure 13). This angle in the wrong strategy is 25° (Figure 14). This case indicates that BH-3 borehole will cut most discontinuity along the shear zone at the right strategy. This case also affect the values of discontinuity frequency and spacing along the boreholes.

In situations in which there is no knowledge of the discontinuities to be encountered during subsurface exploration, the best strategy is to select a combination of different borehole orientations that minimizes the changes that the average orientation of any discontinuity set falls into a Terzaghi (1965) blind zone.

### Bearing Capacity Analyses Performed by Using the Equations Considering the RQD Value

Discontinuity numbers were counted along the borehole profiles. Thus, the value of discontinuity frequency ( $\lambda$ ) and spacing ( $d$ ) were computed for each core run. Variations of the fracture frequency ( $\lambda$ ), spacing ( $d$ ), RQD %, CR %, and core loss (CL % = 100 – CR %) with depth along the borehole profiles are presented in Figure 15. Zones where the core loss is greater than 30% are observed in three levels located at the different depths of the boreholes (Figure 15). These zones are located in the highly-weathered gneisses. The increase of fracturing in these zones (weakness zones) relative to the adjacent rock is up two to three times (as revealed by the core logs). These zones are as follows; in the BH-1, zone-I: 0-8 m, zone-II: 14- 22 m, and zone-III: 23.40-28 m; in the BH-2, zone-I: 0 -7.40 m, zone-II: 10.50-18.70 m, and zone-III: 25-30 m; in the BH-3, zone-I: 0 - 9.50 m, zone-II: 15.50-17.50 m, and zone-III: 21.50-25.50 m. If these zones mentioned above are correlated, they appear to exist in the three weakness-zones in the gneisses trending in NE-SW direction. The weakness zones both in the gneiss unit and in the contacts between the geological units are shown in the A-A', C-C', and E-E' cross-sections (Figure 4). It is determined that the geological structure, which has a large lenticular mass similar to a salt plug, rose towards the surface and the weakness zones in terms of the fracture intensity. Weakness





BH-2 borehole does not cut the shear zone. It should be noted that the great circle of shear zone (70/290) fall into the blind zone of BH-2 borehole (acute angle : 5°). BH-3 borehole however, cut very few numbered discontinuity along the zone.

Figure 14. The wrong drilling strategy and its lower hemisphere (If the shear zone had been inclined to the NW direction, BH-3 borehole would intersect very few numbered discontinuity).

Şekil 14. Yanlış sondaj stratejisi ve ona ait alt yarım küre projeksiyonu (Makaslama zonu KB'ya eğimli olsaydı BH-3 sondajı çok daha az sayıda süreksizlik keserdi).

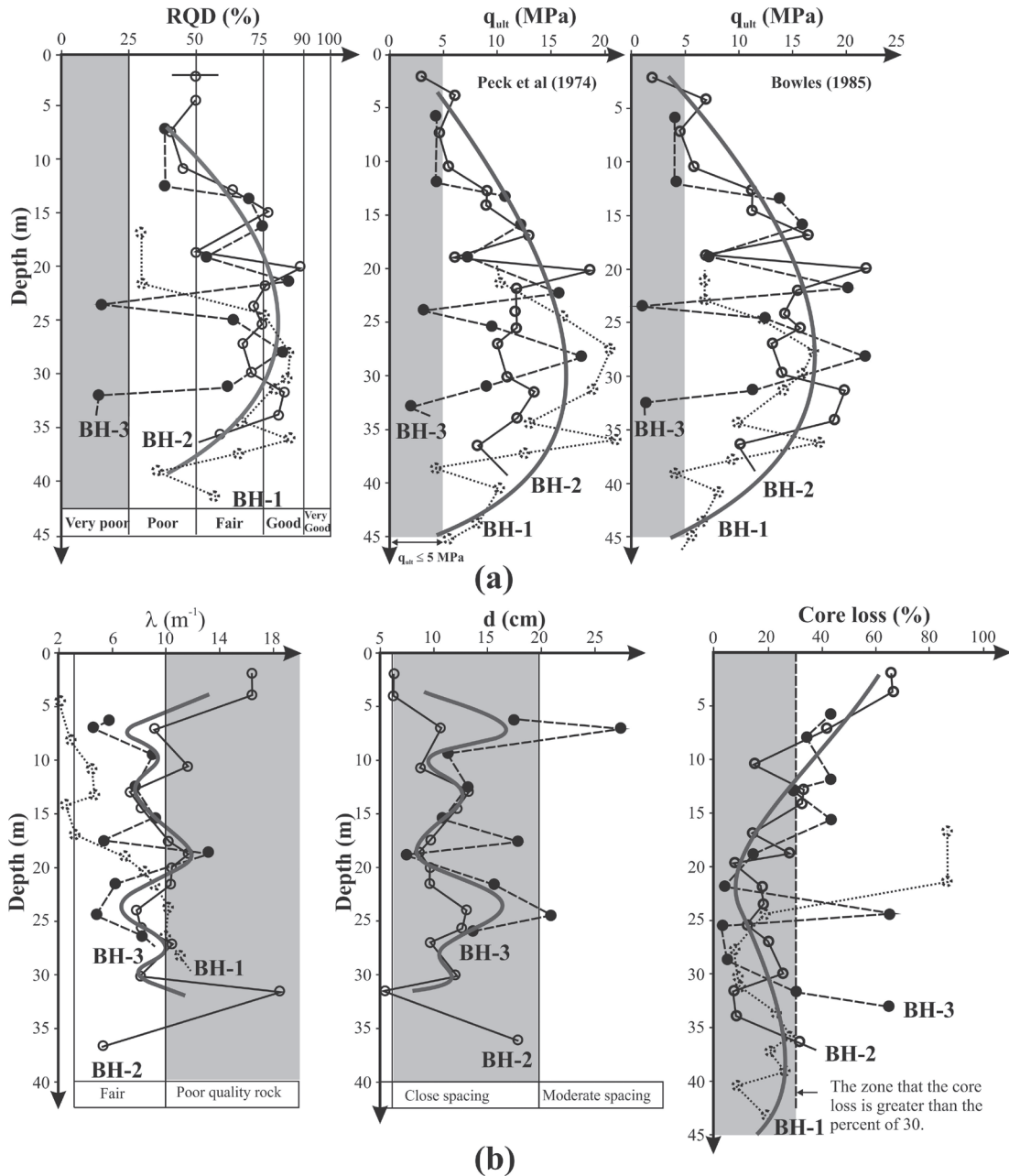


Figure 15. (a) Variations of the RQD% values and ultimate bearing pressures ( $q_{ult}$ ) with depth (The zones which the  $q_{ult}$  is lesser than 5.0 MPa, is gray coloured), (b) Variations of the fracture frequency ( $\lambda$ ), spacing ( $d$ ), and core loss (%) with depth along the borehole profiles (The depth of platform in BH-3 on which the plant will be constructed is 6.63 m. These depths in BH-1 and BH-2 are 2.525 m. and 3.08 m, respectively).

Şekil 15. (a) Derinlikle nihai taşıma gücü ve RQD değerlerinin derinlikle değişimi ( $q_{ult} < 5.0$  MPa olan zonlar gri renklidir), (b) sondaj profilleri boyunca karot kaybı, süreksizlik aralığı ve sıklığının derinlikle değişimleri (Üzerine tesisin inşa edileceği platformun derinlikleri; BH-3, BH-1 ve BH-2 sondajlarında sırasıyla 6.63 m, 2.525 m ve 3.08 m'dir).

Determination of this structure is of utmost importance both for the mining operations and for the determination of the bearing capacity zone. It is thought that bearing capacity problems will occur due to the existence of the tectonic zone with heavily-jointed rock properties (close spacing and poor quality rock) and the contacts between the geological units including the sheared surfaces. These surfaces are clearly observed in the cut-slope face located in the southern part of the plant area (Figure 5). As expected, shear strength along the shear surfaces are very low or nearly zero due to the lack of cohesion along these surfaces. For BH-1, BH-2 and BH-3 boreholes, the results of computations of the allowable bearing pressure of gneisses are

presented in Tables 8, 9, and 10, respectively. The results obtained from different geotechnical methods are also reported in these tables. The foundation pressure of the bunker is 0.51 MPa on the ground surface. The zones which are under this value are given above in terms of the bearing capacity: in the BH-1, 0-4.10 m; in the BH-2, 0-7.40 m; and in the BH-3, 15.50-17.50 m and 24.50-25.50 m. In these zones, core losses reach the maximum values (Figure 15). The general trend in the graph of the variation of RQD-values with depth is similar to the graph of the normal distribution. The variation of ultimate bearing pressure with depth is also seen in this graph (Figure 15).

Table 8. Bearing capacity values obtained from different equations along the BH-1 borehole (z: 461.02 m, platform base of the plant: 458.15 m).

Çizelge 8. BH-1 sondajı boyunca farklı derinlikler için farklı eşitliklerden elde edilen taşıma gücü değerleri.

Depth (m)	RQD (%)	$q_u$ (kg/cm <sup>2</sup> )		The methods considering the RQD% value			$q_a$ (MPa) Suggested Allowable Bearing Pressure ( $q_a = q_{ult}/F_s$ )	
		Depth (m)	$q_u$	$q_{ult}$ (MPa) Peck et al. (1974)	$q_{ult}$ (MPa) Bowles (1988)	$q_{ult}$ (MPa) Bowles (2001)	$F_s = 3$	$F_s = 6$
4.10-4.80	61.0	-	-	10.4	7.10	-	1.1	2.2
4.80-7.80	75.6	5.10	190	15.98	12.3	10.8	1.8	3.6
7.80-10.70	85.7	8.50	235	20.5	16.7	17.2	2.3	4.6
10.7-13.25	84.3	12.0	268	19.8	16.0	19.0	2.65	5.3
13.25-14.1	80.0	-	-	17.9	14.0	-	2.33	4.67
14.1-17.20	67.7	-	-	12.8	9.8	-	1.65	3.3
17.2-18.80	86.6	18.3	242	20.9	17.4	18.1	2.4	4.8
18.8-20.30	66.6	-	-	12.4	9.5	-	1.6	3.2
20.3-21.75	35.8	-	-	3.58	4.0	-	0.6	1.2
21.75-23.4	58.8	-	-	9.6	7.7	-	1.3	2.57
23.4-26.50	52.9	25.4	150	7.8	6.5	4.90	0.81	1.63
26.5-28.10	46.2	-	-	5.9	5.5	-	0.91	1.83

\*: 0.0-4.10 m: sediment sample.

Table 9. Bearing capacity values obtained from various equations along the BH-2 borehole (z: 478.03 m, platform base of the plant: 475.00 m).

Çizelge 9. BH-2 sondajı boyunca farklı derinlikler için farklı eşitliklerden elde edilen taşıma gücü değerleri.

Depth (m)	RQD (%)	$q_u$ (kg/cm <sup>2</sup> )		The methods considering the RQD% value			$q_a$ (MPa) Suggested Allowable Bearing Pressure	
		Depth (m)	$q_u$	$q_{ult}$ (MPa) Peck et al. (1974)	$q_{ult}$ (MPa) Bowles (1988)	$q_{ult}$ (MPa) Bowles (2001)	$F_s = 6$	$F_s = 3$
2.25 – 4.0	27.0	-	-	2.85	2.03	-	1.1	0.55
4.0 – 4.3	50.0	5.0	204	6.00	6.99	5.10	2.0	1.00
4.3 – 7.0	41.0	6.5	190	4.73	4.70	3.20	1.1	0.55
7.0 – 10.5	45.3	-	-	5.34	5.74	-	1.8	0.90
10.5 – 12.5	63.7	11.5	218	8.80	11.35	8.84	2.4	1.20
12.5 – 14.5	63.3	-	-	8.70	11.20	-	2.9	1.45
14.5 – 16.5	77.1	-	-	12.82	16.62	-	4.3	2.15
16.5 – 18.5	50.5	-	-	6.15	7.13	-	2.0	1.00
18.5 – 20.0	89.0	18.0	300	18.6	22.15	23.7	6.0	3.00
20.0 – 22.0	74.5	-	-	11.9	15.52	-	4.0	2.00
22.0 – 23.5	72.0	-	-	11.09	14.50	-	3.7	1.85
23.5 – 25.0	74.4	25.0	230	11.87	15.48	12.7	4.0	2.00
25.0 – 27.0	68.5	-	-	10.05	13.12	-	3.3	1.65
27.0 – 30.0	71.1	26.8	188	10.80	14.14	9.50	3.2	1.60
30.0 – 31.5	84.0	-	-	15.83	19.73	-	5.3	2.65
31.5 – 34.0	81.1	-	-	14.45	18.40	-	4.8	2.40
34.0 – 36.5	59.9	35.4	206	7.93	10.04	7.40	2.3	1.15

\*: Loss of core in the marked zones is greater than the percent of 17.  $F_s$ : Factor of safety

Table 10. Bearing capacity values obtained from the various equations along the BH-3 borehole (z: 472.04 m, platform base of the plant: 462.50 m).

Çizelge 10. BH-3 sondajı boyunca farklı derinlikler için farklı eşitliklerden elde edilen taşıma gücü değerleri.

Depth (m)	RQD (%)	q <sub>u</sub> (kg/cm <sup>2</sup> )		The methods considering the RQD% value			q <sub>a</sub> (MPa) Suggested allowable bearing pressure	
		Depth (m)	q <sub>u</sub>	q <sub>ult</sub> (MPa) Peck et al. (1974)	q <sub>ult</sub> (MPa) Bowles (1988)	q <sub>ult</sub> (MPa) Bowles (2001)	F <sub>s</sub> = 6	F <sub>s</sub> = 3
0.00 - 6.0	39.25	-	-	4.51	4.29	-	1.45	0.72
6.00 - 7.0	71.00	8.00	196	10.77	14.0	9.9	2.8	1.40
7.00-9.50	75.60	-	-	12.25	15.90	-	4.0	2.00
9.50-12.50	55.70	-	-	7.09	7.33	-	2.3	1.15
12.5-15.50	85.00	-	-	16.34	20.10	-	5.4	2.70
15.50 - 17.5	17.00	-	-	3.08	1.00	-	0.7	0.35
17.5-18.50	67.00	-	-	9.63	12.50	-	3.2	1.60
18.50-21.50	88.30	-	-	18.25	21.70	-	6.0	3.00
21.50 - 24.5	63.00	22.50	182	9.0	11.07	7.2	2.0	1.00
24.50 -25.5	16.00	-	-	2.14	0.71	-	2.4	1.20

F<sub>s</sub>: Factor of safety

Bearing capacity values and stresses induced by surcharge loads were determined for the metamorphic rocks in the site. In addition, the significant depth under the platform base is very important from the bearing capacity point of view. For this reason, the values of bearing capacity in the depth known as the bearing capacity zone, and generally changing from the ground surface level to the depth of 0.0 - 6.0 m, are of utmost importance for rock mass. If the geologic and geotechnical data obtained from the borehole BH-1 are considered, the results given as follows regarding bearing capacity analyses are reached: the platform of the plant at this point is located at a depth of 2.85 m from the ground surface level (the elevation of this depth is +458.5 m). The minimum allowable bearing pressure was determined as  $q_{a \min} = 590$  kPa in the zone between +440.7 and +439.2 m elevations (Figure 4). This zone is located at 17.45 m below

the platform base of the plant. If the data from the borehole BH-2 are considered, the results related to the bearing capacity analyses given as follows are reached: the platform of the plant at this point is located at a depth of 3.08 m. below the ground surface level (the elevation of this depth is +475 m). The minimum allowable bearing capacity value was determined as  $q_{a \min} = 530$  kPa in the zone between +473.3 and 470.6 m elevations. If the data from the borehole BH-3 are considered, the results of relations to the bearing capacity analyses given as follows are reached: the platform base of the plant at this point is located at the elevation of +462.5 m. The minimum allowable bearing pressure was determined as  $q_{a \min} = 350$  kPa in the zone between +465.5 and +454.5 m. elevations. This zone starts 6.0 m. below the platform base, and its thickness is approximately 2.0 m.



Table 11. The input and output parameters used in numerical analysis by means of Generalized Hoek-Brown Criterion.

Çizelge 11. Genelleştirilmiş Hoek-Brown Ölçütü yardımıyla nümerik analizlerde kullanılan yazılım girdi ve çıktıları.

Rock Type	Intact Rock Properties		D	Rock Mass Properties				
	(Dilation parameter: 0 Unit Weight: 0.024 MN/m <sup>3</sup> )			(Poisson's ratio: 0.23)				
Tectonic Zone	$m_i$	$\sigma_{ci}$ (MPa)	0.7	GSI	s	a	$m_b$	$E_{rm}$ (MPa)
	11	10		31	$4.47 \times 10^{-6}$	0.561	0.103	130

GSI: Geological strength index;  $m_i$ : Hoek-Brown constants for intact rock material;  $m_b$ , s, a: Hoek-Brown constants for rock mass; D: disturbance factor

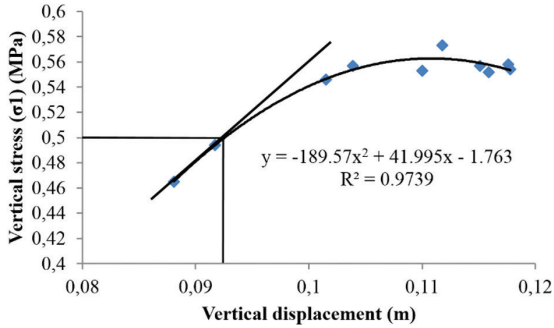


Figure 17. The plot of vertical stress to vertical displacement for the line at 2 m depth under the foundation of bunker.

Şekil 17. Kırıcı besleme noktasına ait temelin 2 m altında hat boyunca düşey gerilme-düşey yer değiştirme ilişkisi.

Figure 17 indicates that there is strong polynomial relationship between the vertical stress and vertical displacement beneath the foundation of the bunker. Fundamentally, this relationship shows a linear trend until a point which the trend becomes non-linear. Theoretically, this point can be assumed to be the ultimate bearing capacity of the rock mass. Consequently, it was

determined that the ultimate bearing capacity of the rock mass is 500 kPa where the vertical displacement is 0.092 m. The allowable bearing capacity is therefore 167 kPa ( $F_s: 3$ ) which is significantly lower than the ones calculated from geophysical and geotechnical data. The bearing capacity of rock mass will not respond and thus, settlement at a certain level (0.092 m) will occur in the rock mass. It can also be revealed that the allowable bearing capacity values derived from the numerical analysis is more conservative than the ones from other methods.

## Geophysical Survey

Determination of the extent of the weakness zones in the lateral direction into the metamorphic rock mass was performed using the speed of P-wave velocity ( $V_p$ ) for the line-I (Figure 18). The existence of four weakness-zones controlled by the discontinuities with nearly vertical position in this line was determined (Figure 18). Thus, a dome-like geological structure developed in the metamorphic rock mass was confirmed by the geophysical survey.

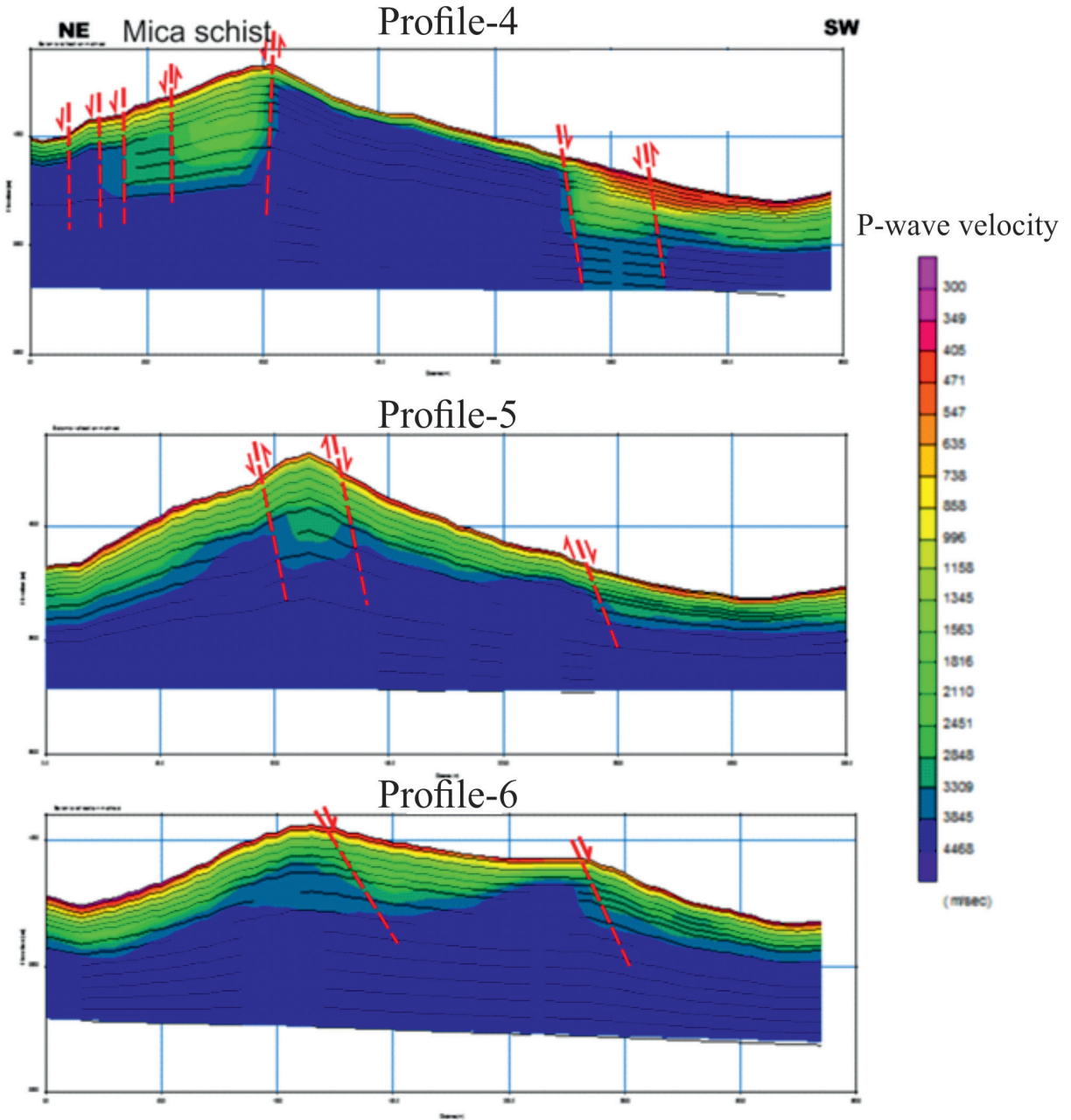


Figure 18. Determination of the weakness zones in lateral direction into the rock mass using  $V_p$  determined from the geophysical measurement line-1.

Şekil 18. Jeofizik ölçüm hattı-1 için  $V_p$  değerleri kullanılarak kayaç kütleindeki yatay yöndeki zayıflık zonlarının belirlenmesi.

This situation makes the study a little interesting. A zone where  $V_p$  is less than 900 m/sec exists in the upper elevations of the topographic profile in Figure 18. The thickness of the zone (the colour of which is red) increases towards to the stream due to the water effect and tectonic. This zone with low  $V_p$ -velocity is located in the gneiss unit. It is determined that the yellow and red coloured zones with relatively low P-wave velocities ( $V_p < 800$  m/sec) and 5-7 m thicknesses are located at the western part of line-I. This zone generally exists under + 490 and +485 m elevations. The green coloured zone represents the rock mass that is stronger than the others in terms of the bearing capacity (Figure 18). The graph showing the changes of Vs-shear wave velocities with depth and the bearing capacity zones for the geophysical measurement line-I is given in Figure 19.

$V_s$ -values in the line-I were measured at 825 and 940 m/sec. However,  $V_s$ -values decrease slightly at the eastern part of the line-I. Although a little difference in the  $V_s$ -values was obtained, two bearing pressure zones were distinguished in the line-I (Figure 19). A zone with relatively low  $V_s$ -values ( $830 \leq V_s \leq 870$  m/sec) at the western part of the line-II is determined from the geophysical measurements. This zone is located between +483 m. and +495 m. elevations in the gneisses and the tectonic zone. The zone with relatively low  $V_p$ -velocities ( $1020 \leq V_p \leq 1130$  m/sec) increases as it goes towards the stream, Another zone exists as a pocket between +460 m and +470 m elevations on the eastern side of line-3. Minimum  $V_s$ -values (650 m/sec) and bearing capacity values were measured in this zone (Table 12 and Figure 19). Allowable bearing pressures for zone-I and zone-II (along line-I, line-II, and line-III) are computed using the values of  $V_p$  and  $V_s$ , and their results are presented in Table 12.

Table 12. Allowable bearing capacity values ( $q_{all}$ ) obtained using the P and S-wave velocities along the geophysical measurement lines (I, II, and III). For the calculation of  $q_{all}$ -values, Equation-9 was used.

Çizelge 12. Jeofizik ölçüm hatları boyunca P ve S dalga hızları kullanılarak elde edilen izin verilebilir taşıma gücü değerleri.

Section No	Geophysical parameters	Zone-I	Geophysical parameters	Zone-II
Section-I	$V_{p1}$ (m/sec)	1540 - 1411	$V_{p2}$ (m/sec)	1600
	$V_{s1}$ (m/sec)	904-826	$V_{s2}$ (m/sec)	940
	$\gamma_{n1}$ (kN/m <sup>3</sup> )	24.1	$\gamma_{n2}$ (kN/m <sup>3</sup> )	24.1
	$S_v$	0.956	$S_v$	0.949
	$q_a$ (MPa)	5.0	$q_a$ (MPa)	5.16
Section- II	$V_{p1}$ (m/sec)	1651	$V_{p2}$ (m/sec)	1899
	$V_{s1}$ (m/sec)	965	$V_{s2}$ (m/sec)	996
	$\gamma_{n2}$ (kN/m <sup>3</sup> )	24.5	$\gamma_{n2}$ (kN/m <sup>3</sup> )	24.7
	$S_v$	0.944	$S_v$	0.938
	$q_a$ (MPa)	5.25	$q_a$ (MPa)	5.54
Section-III	$V_{p1}$ (m/sec)	1253	$V_{p2}$ (m/sec)	1565
	$V_{s1}$ (m/sec)	720 - 650	$V_{s2}$ (m/sec)	910
	$\gamma_{n3}$ (kN/m <sup>3</sup> )	22.8	$\gamma_{n3}$ (kN/m <sup>3</sup> )	24.16
	$S_v$	0.983-0.99	$S_v$	0.954
	$q_a$ (MPa)	3.87-3.52	$q_a$ (MPa)	5.0
Average value		$\bar{X} = 4.70$ MPa		$\bar{X} = 5.23$ MPa

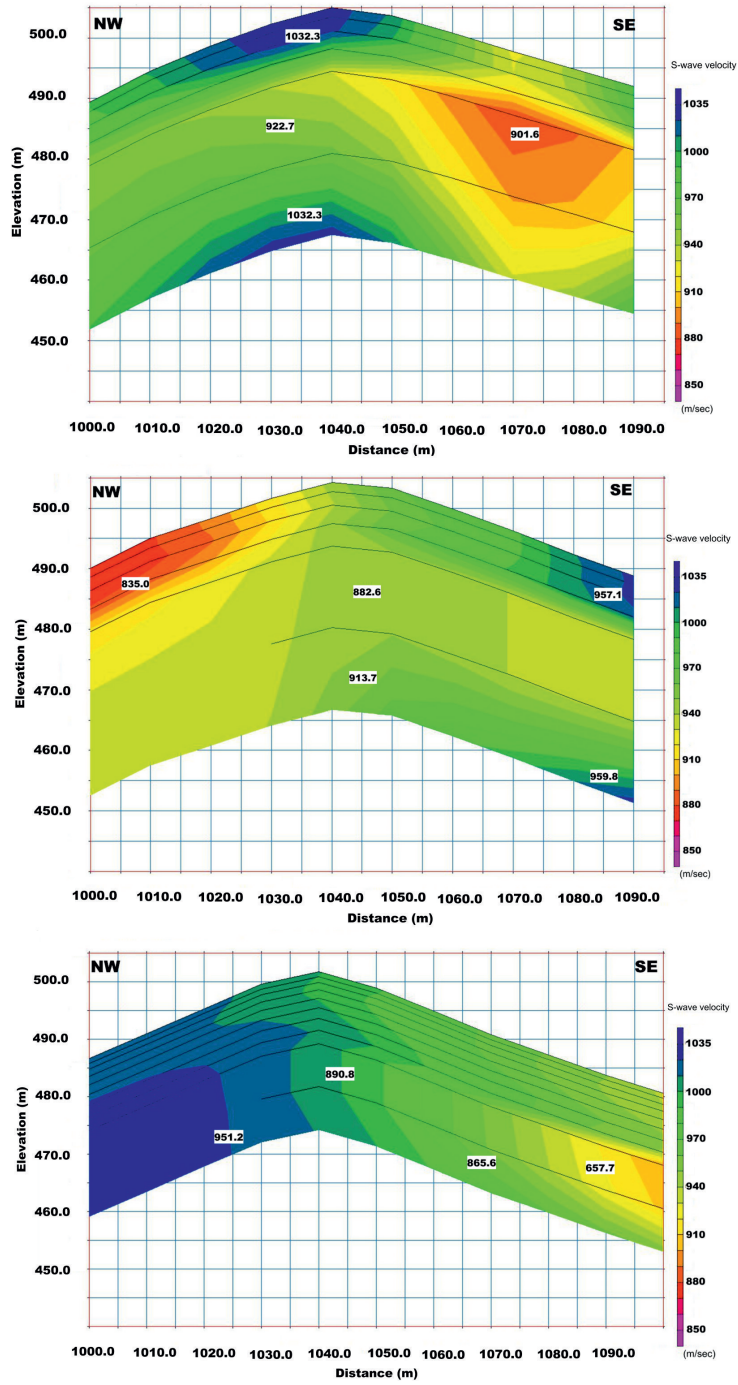


Figure 19. The graphs showing the change of  $V_s$ -values with depth and the bearing capacity zones for the geophysical measurement lines (line-I, line-II, and line-III).

Şekil 19. Jeofizik ölçüm hatları için taşıma gücü zonları ve derinlikle S-dalga hızlarının değişimini gösteren grafikler.

## DISCUSSIONS AND CONCLUSIONS

The geotechnical site investigation was performed, considering the geotechnical data acquired during the scan-line works, geophysical survey, and three inclined boreholes. Based on this data, it was confirmed by the current study existing of the geological structure observed at the plant site is a dome-like structure. This structure has a large lenticular mass similar to a salt plug that rose towards the surface, and is laid along the NE-SW direction. In addition, the ore body is covered as a strip by the tectonic zone. This structure was also confirmed by the geophysical survey.

The acute angles between the shear zone and the axes of the drill holes BH-3, BH-2, and BH-1 were determined as 65°, 35°, and 31°, respectively using the stereographic projection techniques. The acute angles for the foliation planes were also determined as 16°, 40°, and 44°, respectively. The plunge angle of borehole BH-3 is quite close to the dip angles (26° - 42°) of the foliations. The acute angle between the strikes of the foliations and the axis of the borehole was determined as 16°. This case decreased the probability of BH-3 borehole intersect the foliation planes considerably. On the other hand, foliations are intersected along the BH-1 and BH-2 boreholes mostly. It was determined that BH-2 and BH-1 boreholes intersected the shear zone mostly and to some lesser degree the foliation planes. On the other hand, it was also determined that the boreholes did not intersect the discontinuity sets of 1, 2, and 3 due to the acute angles among them.

RQD (%), CR (%),  $\lambda$  (m<sup>-1</sup>),  $s$  (m), and core loss (%) were determined from the geotechnical logs. Acute angles between the axes of the BH-2 and BH-1 drill holes and the foliation planes were found to be as 40° and 44°, respectively. In order

to compute the true fracture frequency ( $\lambda'$ ) for each length of core advance along the boreholes, the acute angles were used in the computations ( $\lambda' = \lambda \times \text{Cos}\alpha$ ). On the other hand, the acute angle between the strikes of the foliation and the axis of the BH-3 borehole was determined as 16°. It was seen that this case decreased the probability of BH-3 borehole cut the foliation planes as limited. However, it was found that BH-3 borehole intersected the discontinuities belonging to the joint set 4, and the shear zone. For this reason, the acute angles between the axis of the BH-3 borehole and other discontinuity sets were not considered in the computations of  $\lambda$ . Number of discontinuity was directly counted for each length of core advance and that value was considered.

It was determined that the bearing capacity values obtained from the geotechnical computations ( $q_a$ -values computed in the case where the factor of safety is equal to 3) almost agree with the ones acquired from the geophysical measurements. Except the weakness zones determined in this work, no significant problem is predicted to take place at the site (Figure 20). The average value of  $q_a$  for the zone at 16.2 m depth is obtained as 400 kPa when the first 4.1 m and last 8 m are excluded in BH-1. When the weakness zone in the first 7.4 m depth is not taken into account, the  $q_a$ -value is derived as 357 kPa at 28.9 m depth. The location of BH-3 is composed of highly weathered gneiss under the influence of a stream bed. Therefore, the weakness zones in BH-3 are more frequent than those of the other boreholes. When the weakness zones between 0-6.0 m and 15.5-17.5 m are not considered,  $q_a$  is obtained as 351 kPa. On the contrary, the allowable bearing capacity values obtained from the geotechnical computations do not agree well with the one obtained from numerical modelling by using factor of safety as

3. However, if the factor of safety is used as 6 in ultimate bearing capacity obtained from the geotechnical calculations, the results would be more comparable with the numerical modelling.

$\geq 900$  m/sec. The value of 900 m/sec is nearly the limit value of the rocky formations. The  $V_s$ -values between 500 m/sec and 900 m/sec can be admitted as “a transition zone” between

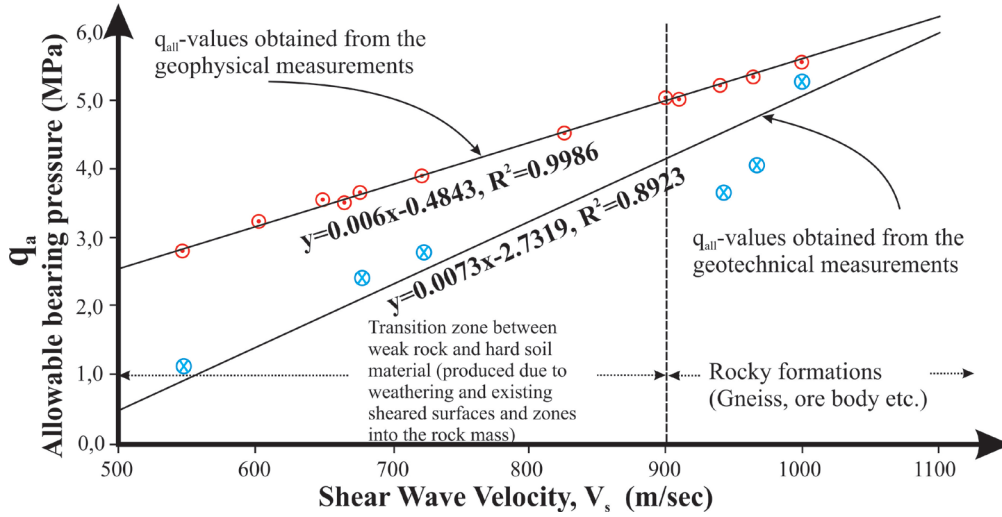


Figure 20. Relationships between the shear wave velocities ( $V_s$ ) and  $q_a$ -values, and the variation of the  $q_a$ -values based on the geotechnical measurements at depths where the geophysical measurements were performed.

Şekil 20. Jeofizik ölçümlerinin yapıldığı derinliklerdeki jeoteknik ölçümler üzerine temellendirilmiş izin verilebilir taşıma gücü değerlerinin ( $q_a$ ) değişimi ve  $q_a$  değerleriyle  $V_s$  - değerleri arasındaki ilişkiler.

It is determined that the bearing capacity problems may take place due to the existing tectonic zone (shear zone) with heavily-jointed structure. The contacts between the geological units including sheared surfaces with nearly vertical position may also adversely affect bearing capacity. Some of the plant units such as the bunker and concrete berm wall should not be constructed on these zones. The  $q_a$ -values obtained from the  $V_s$ -values based on the geophysical measurements and the geotechnical parameters based on the geotechnical measurements within the same depths are correlated with one another (Figure 20). It is seen from the graph that as the shear wave velocities of the rocks increase,  $q_a$ -values also increase. Two lines seen on the graph in this figure draw near to one another after  $V_s$

weak gneissic rocks and very hard to hard soil materials produced by weathering and existing sheared surfaces, and zones into the gneissic rock mass. As a result, it was determined that the  $q_a$ -values based on the geotechnical works are more conservative than the ones from the geophysical measurements. When all results are considered, the ratio between the bearing capacity values acquired from geotechnical and geophysical measurements is close to 0.65.

The maximum contact stress underneath the foundations of the plant units is expected to be on the order of 510kPa. This stress will be transferred to the supporting rock by the foundation of the bunker. The foundation of the bunker is located on different rock units with different varying properties. These units are:

tectonic zone including sheared discontinuity surfaces into the gneiss, and ore body. The location of the bunker should be switched to the BH-1 and/or BH-2 borehole locations due to the above-mentioned reasons. Smaller contact stresses are 0.43 MPa from the concrete berm and 0.29 MPa from the mill. The above mentioned units will be placed on the flat platforms to be generated as a result of 2 to 26 m deep excavations. Therefore, near the ground, highly-weathered zones that contain wide cracks will be excavated. Considering the platform elevations, the estimated safe bearing capacity values were found to be generally satisfactory. It was noticed that bearing capacity values could be as low as 350 kPa in densely fractured zones (i.e. tectonic zone), and in the zones containing mica. Besides, the numerical analysis yielded an allowable bearing capacity of 167 kPa for the first 2 m depth below the ground surface in the tectonic zone. The above mentioned bearing capacity estimations are based on the consideration that there would be no voids and open fractures underneath the flat platforms to be generated as a result of the projected excavation work. On the other hand, it was determined that the allowable bearing capacity values derived from the numerical analysis performed by using the software is more conservative than the ones from other methods. As the vertical stress applied on the rock mass by means of bunker considered, the bearing capacity of the rock mass will not respond and thus, settlement up to 0.092 m will occur. For this reason, the material with 2 m thickness under the foundation of bunker should be excavated.

## REFERENCES

- ASTM D 2113, 1990. Standard Practice for Rock Core Drilling and Sampling of Rock for Site Exploration. Vol: 04.08. American Society for Testing and Materials, Philadelphia, PA, pp. 2113-2114.
- Bowles J. E., 1988. Foundation Analysis and Design. 4<sup>th</sup> Ed. McGraw-Hill Book Company, Singapore, p. 1175.
- Bowles J. E., 2001. Foundation Analysis and Design. 5<sup>th</sup> Ed. Mc Graw-Hill Inc., US, p. 1181.
- Dips 6.0, 2015. Rocscience Inc., <https://www.rocscience.com>.
- El-Naga A., 2004. A comparative review in regards to estimating bearing capacity in jointed rock masses in northeast Jordan. Bulletin of Geoenvironmental Engineering 63:233-245.
- Haneberg W.C., 2009. Improved optimization and visualization of drilling directions for rock mass discontinuity characterization, Environmental Engineering Geology Vol. XV, No. 2, May 2009, 107-113.
- Hoek, E. Carranza Torres, C. Corkum, B. 2002. Hoek & Brown criterion, 2002 Edition. North American Rock Mechanics Symposium, Toronto, Canada, 1, 267-273.
- Hudson, J.A., Priest, S.D., 1979. Discontinuities and rock mass geometry, International Journal of Rock Mechanics and Mining Sciences and Geomechanics Abstracts 16, 339-362.
- Hunt, R. E., 2005. Geotechnical Engineering Investigation Handbook. Second Ed., Taylor & Francis, New York, p. 1081.
- International Society for Rock Mechanics (ISRM), 2007. The Complete ISRM Suggested Methods for Rock Characterization, Testing and Monitoring: 1974-2006, In: Ulusay R and Hudson JA (Editor), Ankara/Turkey.

- Kadakci T., 2011. Slope Stability Assessment of the Open Pit Albite Mine in the Çine-Karpuzlu (Aydın) Area. Dissertation, Graduate School of Natural and Applied Sciences of Dokuz Eylül University.
- Koca, M.Y., Özden G., Kıncaç C., 2014. The Geotechnical Site Investigation Report For The Site of The Crushing, Grinding and Flotation Plant in Karpuzlu-Çine (Aydın). Dokuz Eylül University Research report, June-2014, p. 91, İzmir.
- Martel, S.J., 1999. Analysis of fracture orientation data from boreholes, *Environmental and Engineering Geoscience*, Vol. V, No. 2, 213-233.
- Merifield, R. S., Lyamin, A. V. Sloan, S.W. 2006. Limit analysis solutions for bearing capacity of rock masses using the generalized Hoek & Brown criterion, *International Journal of Rock Mechanics and Mining Sciences* 43, 920-937.
- Micromine, 2014. v.15.0.4 software manual, <http://www.micromine.com>.
- Palmer D., 2001. Imaging refractors with the convolution section. *Geophysics*. 66 (5):1582–1589.
- Peck R.B., Hanson W.E., Thornburn T.H., 1974. *Foundation Engineering*. John Wiley & Sons Inc. New York.
- Rocscience, 2010. Phase 2 version 7.0. Two dimensional finite element analysis program. Rocscience Inc.
- Priest, S.D., 1994. *Discontinuity Analysis for Rock Engineering*, Chapman & Hall, London, 473 p.
- Saada, Z., Maghous, S. Garnier, D., 2008. Bearing capacity of shallow foundation on rocks obeying a modified Hoek&Brown criterion, *Computers and Geotechnics*, 35, 144-154.
- Stavropoulou, M., 2014. Discontinuity frequency and block volume distribution in rock masses. *International Journal of Rock Mechanics and Mining Sciences*, 65, 62-74.
- Terzaghi R. D., 1965. Sources of error in joint surveys: *Geotechnique*, Vol. 15, pp. 287-304.
- Tezcan S.S., Keçeli A., Özdemir Z., 2006. Allowable bearing capacity of shallow foundations based on shear wave velocity, *Geotechnical and Geological Engineering* 24:203–218.
- Zhou, W., Maerz, N.H., 2002. Identifying the optimum drilling direction for characterization of discontinuous rock. *Environmental Engineering Geoscience*, Vol. 8, No. 4, 295-307.

